NASA TECHNICAL NOTE

NASA TN D-8473

EFFECT OF WINGLETS ON A FIRST-GENERATION JET TRANSPORT WING

I - Longitudinal Aerodynamic Characteristics of a Semispan Model at Subsonic Speeds

Peter F. Jacobs and Stuart G. Flechner
Langley Research Center
Hampton, Va. 23665

and

Lawrence C. Montoya
Dryden Flight Research Center
Edwards, Calif. 93523

NATIONAL AERONAUTICS AND SPACE ADMINISTRATION • WASHINGTON, D. C. • JUNE 1977

1. Report No. NASA TN D-8473	2. Government Accession No.
4. Title and Subtitle EFFECT OF WINGLETS ON A FIRST-GENERATION JET TRANSPORT WING. I - LONGITUDINAL AERODYNAMIC CHARACTERISTICS OF A SEMISPAN MODEL AT SUBSONIC SPEEDS	5. Report Date June 1977 6. Performing Organization Code
7. Author(s) Peter F. Jacobs, Stuart G. Flechner (Langley Research Center), and Lawrence C. Montoya (Dryden Flight Research Center)	8. Performing Organization Report No. L-11354
9. Performing Organization Name and Address NASA Langley Research Center Hampton, VA. 23665	10. Work Unit No. 505-11-16-08 11. Contract or Grant No.
12. Sponsoring Agency Name and Address National Aeronautics and Space Administration Washington, D.C. 20546	13. Type of Report and Period Covered Technical Note 14. Sponsoring Agency Code
15. Supplementary Notes	

16. Abstract

Longitudinal aerodynamic characteristics and cross-flow velocity vectors behind the wing tip of a first-generation jet transport semispan model are presented at subsonic speeds. Data are given for the basic wing and configurations with an upper winglet only, upper and lower winglets, and a simple wing-tip extension. To simulate second-segment-climb lift conditions, leading- and/or trailing-edge flaps were added to some configurations.

17. Key Words (Suggested by Author(s)) Winglets Induced drag Drag due to lift Aerodynamic drag reduction	18. Distribution Statement Unclassified - Unlimited Subject Category 02

19. Security Classif. (of this report)	20. Security Classif. (of this page)	21. No. of Pages	22. Price*
Unclassified	Unclassified	48	$4.00

* For sale by the National Technical Information Service, Springfield, Virginia 22161

EFFECT OF WINGLETS ON A FIRST-GENERATION JET TRANSPORT WING

I - LONGITUDINAL AERODYNAMIC CHARACTERISTICS OF A SEMISPAN MODEL AT SUBSONIC SPEEDS

Peter F. Jacobs and Stuart G. Flechner
Langley Research Center

Lawrence C. Montoya
Dryden Flight Research Center

SUMMARY

This paper presents the effects of winglets and a simple wing-tip extension on the aerodynamic forces and moments and the flow-field cross-flow velocity vectors behind the wing tip of a first-generation jet transport wing. The investigation was conducted in the Langley 8-foot transonic pressure tunnel using a semispan model. The test was carried out at Mach numbers of 0.30, 0.70, 0.75, 0.78, and 0.80. At a Mach number of 0.30, the configurations were tested with combinations of leading- and trailing-edge flaps.

Results of the investigation indicate that the winglets reduce induced drag by approximately 20 percent at cruise conditions. The tip extension, designed to produce wing bending-moment increments at design conditions equivalent to those produced by the winglets, reduces induced drag by 10 percent. The winglets and tip extension produce small negative increments in pitching-moment coefficient; however, the increments associated with the addition of the winglets are less than those produced by the tip extension. At cruise conditions, the winglets and tip extension produce positive increments in lift-drag ratio of 9 percent and 4 percent, respectively. At a second-segment-climb Mach number of 0.30, the winglets continue to be more aerodynamically efficient than the tip extension. Configurations with the upper winglet only, upper and lower winglets, and the tip extension produce increases in lift-drag ratio of 10 percent, 9 percent, and 6.5 percent, respectively, at a lift coefficient near 1.0.

INTRODUCTION

Winglets, as described in reference 1, are intended to provide reductions in drag coefficient, at cruise conditions, substantially greater than those obtained with a simple wing-tip extension, which has been designed to impose the same bending increments on the wing structure as the winglets. The National Aeronautics and Space Administration has been conducting extensive experimental investigations of the effects of winglets on jet transport wings at high subsonic Mach numbers. (See refs. 2 and 3.)

This investigation was conducted to determine the effects of winglets and a simple wing-tip extension on the longitudinal aerodynamic characteristics, surface static-pressure distributions, and cross-flow velocities behind the wing tip of a first-generation jet transport. This paper, which is one of a series, presents the effects of winglets on the longitudinal aerodynamic characteristics and cross flows only. Chordwise static-pressure distributions and spanwise loadings for the wing and winglets are presented in references 4 and 5. Data were taken at Mach numbers of 0.30, 0.70, 0.75, 0.78, and 0.80. At a Mach number of 0.30, the configurations were tested with combinations of leading- and trailing-edge flaps. To obtain the highest possible Reynolds number, a semispan model was used. The tests were conducted in the Langley 8-foot transonic pressure tunnel.

SYMBOLS

Force and moment data have been reduced to coefficient form based on the exposed trapezoidal area of the basic wing. All dimensional values are given in both the International System of Units (SI) and U.S. Customary Units (ref. 6). All measurements and calculations were made in U.S. Customary Units.

Coefficients and symbols used herein are defined as follows:

b'	exposed semispan of wing with basic tip, 124.26 cm (48.92 in.)
$\Delta b'$	incremental increase in exposed wing semispan (tip extension), 0.38 of span of upper winglet, 7.62 cm (3.00 in.)
c	local chord, cm (in.)
$\bar{c}$	mean geometric chord of exposed basic wing, 39.98 cm (15.74 in.)
c_t	tip chord of basic wing, cm (in.)
$C_{B'}$	bending-moment coefficient at wing-fuselage juncture, Bending moment/$q_\infty Sb'$
C_D	drag coefficient, Drag/$q_\infty S$
ΔC_D	incremental drag coefficient, $C_D - C_{D,basic}$
C_L	lift coefficient, Lift/$q_\infty S$
ΔC_L	incremental lift coefficient, $C_L - C_{L,basic}$
C_m	pitching-moment coefficient, Pitching moment/$q_\infty S\bar{c}$
g	acceleration due to gravity, 980.7 cm/sec^2 (32.2 ft/sec^2)
h	span of the upper winglet from chord plane of wing tip (see fig. 2(b)), cm (in.)

i	incidence of winglet measured from free-stream direction, positive with leading edge inward for upper winglet, outward for lower winglet (see fig. 2(b)), deg
M_∞	free-stream Mach number
q_∞	free-stream dynamic pressure, Pa (psf)
R	Reynolds number per unit length, per m (per ft)
S	exposed trapezoidal area of basic wing, 0.4648 m^2 (5.0034 ft^2)
x	chordwise distance from leading edge, positive aft, cm (in.)
y	spanwise distance from wing-fuselage juncture, positive outboard, cm (in.)
z	vertical coordinate of airfoil, positive upward, cm (in.)
α	angle of attack, deg
η	exposed wing semispan station (based on basic-wing panel), y/b'

Subscript:

basic	reference configuration, model with no wing-tip devices

EXPERIMENTAL APPARATUS AND PROCEDURES

Test Facility

This investigation was conducted in the Langley 8-foot transonic pressure tunnel, a continuous single-return tunnel with a slotted rectangular test section. The longitudinal slots in the floor and ceiling of the test section reduce tunnel wall interference and allow relatively large models to be tested through the subsonic speed range. Controls are available to permit independent variation of Mach number, stagnation pressure, temperature, and dew point. A more detailed description of the wind tunnel is given in reference 7.

Model Description

A 0.07-scale semispan model of the KC-135A transport aircraft was used in this investigation. Photographs of the model in the wind tunnel are shown in figure 1. Drawings of the model are shown in figure 2.

Fuselage.- The fuselage contours closely simulate the full-scale fuselage shape, with the exception of the wheel-well area. An enlargement of this area was necessary to enclose the model mounting apparatus. The fuselage midsection covers the balance and has a slot through which the wing protrudes. (The gap between the wing and fuselage results in unrepresentative absolute values of

axial force. Both lift and drag are influenced by the gap effects on axial force; however, these effects can reasonably be considered systematic and thus affect all wing-tip configurations equally at the same test conditions.) The fuselage is not attached to the balance, but it does rotate with the wing through the angle-of-attack range.

Wing.- The basic wing of the KC-135A model has 7° dihedral and 2° of incidence at the root chord. The wing has no geometric twist. A typical outboard airfoil section is shown in figure 3. The wing thickness ratio varies nonlinearly from 15 percent at the wing-fuselage juncture to 9 percent at the trailing-edge break and then remains constant to the wing tip. The trapezoidal planform of the total wing (extended to the fuselage center line) has a sweep at the quarter-chord of 35°, an aspect ratio of 7.00, and a taper ratio of 0.35. For all data analysis, the reference geometry parameters S, b', and $\bar{c}$ are based on the exposed trapezoidal planform of the basic wing. The model wing stiffness was designed so that the relative model bending deflection at the tip was approximately the same as that for the actual airplane at cruise conditions.

Winglets.- A detailed drawing of the winglets used in this investigation is given in figure 2(b). The winglets employed an 8-percent-thick general aviation airfoil. Winglet airfoil coordinates are presented in table I.

The upper winglet has a span equal to the wing-tip chord, a root chord equal to 65 percent of the wing-tip chord, a leading-edge sweep of 38°, a taper ratio of 0.32, and an aspect ratio of 2.33. The planform area of the upper winglet is 3.8 percent of the exposed trapezoidal planform area of the basic wing. The upper winglet is canted outboard 15° from vertical (75° dihedral) and toed out 4° (leading edge outboard) relative to the fuselage center line. The upper winglet is untwisted and therefore has constant negative geometric incidence across its span. The "upper surface" of the upper winglet is the inboard surface.

The lower winglet has a span equal to 23 percent of the wing-tip chord, a root chord equal to 40 percent of the wing-tip chord, a leading-edge sweep of 52°, a taper ratio of 0.40, and an aspect ratio of 0.82. The planform area of the lower winglet is 0.6 percent of the exposed trapezoidal planform area of the basic wing. The lower winglet is canted outboard from vertical 36° (54° anhedral) and toed in 7° (trailing edge outboard) relative to the fuselage center line. The lower winglet was twisted about its leading edge with 4° washout at the tip. The "upper surface" of the lower winglet is the outboard surface.

To smooth the transition from the wing to the winglets, fillets were added to the inside corners at those junctures and the outside corners were rounded.

Tip extension.- The 7.62-cm (3.00-in.) wing-tip extension (fig. 2(a)) has the same coordinates as the outboard wing section. The span was estimated so that the tip extension produced essentially the same increments in bending moment at the wing-fuselage juncture as the winglets.

Nacelles.- Flow-through nacelles were used with an inlet diameter of 5.64 cm (2.22 in.) and exit diameter of 3.45 cm (1.36 in.). The inlet diameter was main-

tained back to approximately 0.66 of the nacelle length and then tapered linearly to the exit.

Flaps.- Fixed-position leading- and trailing-edge flaps were used to simulate second-segment-climb characteristics. The flaps tested were designed merely to be representative and are not modeled after the actual KC-135A flaps. The leading- and trailing-edge flaps were deflected 120° and 20°, respectively. Flap details are shown in figure 4.

The configurations tested with and without flaps are shown in the following table:

Flaps	Test configuration			
	Basic tip	Upper winglet	Upper and lower winglets	Tip extension
Off	X		X	
Trailing edge	X	X	X	X
Leading and trailing edge	X	X	X	

Boundary-Layer Transition Strips

Boundary-layer transition strips were placed on both surfaces of the wing and winglets. These strips were comprised of a 0.159-cm (0.06-in.) wide band of carborundum grains set in a plastic adhesive. The carborundum grains were sized on the basis of reference 8. The transition strip patterns for the wing and winglets are shown in figure 5.

The transition strips on the lower surface of the winglets were located rearward in an attempt to simulate full-scale Reynolds number boundary-layer conditions (ref. 9). The strips on the upper surfaces of the winglets were located forward to insure transition ahead of the shock wave for the various test conditions.

Test Conditions

Measurements were taken at Mach numbers of 0.30, 0.70, 0.75, 0.78, and 0.80 with the model angle of attack ranging from approximately 4° to 12° at M_∞ = 0.30, and -1° to 7° at all other Mach numbers. Stagnation temperature was maintained at 322 K (120° F) throughout the entire test, and the air was dried until the dew point was sufficiently low to prevent condensation effects. The Reynolds numbers and dynamic pressures at which the data were obtained are presented in the following table:

M_∞	R		q_∞	
	per m	per ft	kPa	psf
0.30	11.68×10^6	3.56×10^6	12	251
.70	18.67	5.69	41	850
.75	17.72	5.40	41	850
.78	17.22	5.25	41	850
.80	16.90	5.15	41	850

Measurements

Force and moment data were obtained using a five-component electrical strain-gage balance. Side-force measurements were not taken. At cruise conditions, two sets of data were taken for each configuration. The difference in drag coefficient of the same configuration for the two sets was about 0.0002. At these conditions, the lift and rolling-moment coefficients differed by less than 0.2 and 0.4 percent, respectively. As in reference 2, these increments are given to indicate the repeatability of the data. An accelerometer attached to the wing mounting block inside the fuselage was used to measure angle of attack. Chordwise static pressures were measured at several semispan stations of the basic wing and winglets and are presented in references 4 and 5.

Boundary-layer visualization photographs were taken utilizing the fluorescent-oil-film flow-visualization technique described in reference 10.

A modified version of a special sting-mounted yaw head rake was used to survey the flow field behind two of the wing-tip configurations. The rake used in the investigation of reference 11 was extended on each end to include an additional static-pressure tube and yaw head. The rake was located approximately 2 wing-tip chords downstream of the wing trailing edge with the rake center slightly above and inboard of the wing tip. Data were taken with the rake located in the vertical, horizontal, and $\pm 45^\circ$ positions for the basic-wing and upper-winglet configurations.

After the yaw head rake data were taken, several total-pressure tubes on the bottom two yaw heads were found to be bent. These tubes were straightened prior to the final calibration of the rake; therefore, the data from these two yaw heads are incorrect and are not presented.

Wing-tip deflections were determined from photographs of a chordwise line on the edge of the wing tip and are presented in references 4 and 5.

The slotted wind-tunnel test section is designed to reduce wall effects on lift. References 4 and 5 show that the wing spanwise load distributions for all configurations at the same conditions are nearly identical over the major portion of the span. Therefore, wall effects on wing lift can be considered systematic, and no correction is made to the data for these effects. The wing semispan and the model frontal area were sufficiently small (1.5 percent of the

test-section cross-sectional area) to avoid having to correct Mach number for wind-tunnel blockage effects (ref. 12).

PRESENTATION OF RESULTS

The results of this investigation are presented in the following figures:

RESULTS AND DISCUSSION

Cruise

During cruise, the KC-135A cargo/tanker aircraft can fly at wing loadings and lift coefficients covering a wide range. For a representative mission, the aircraft may fly at lift coefficients from 0.3 to 0.5 for cruise Mach numbers near 0.78. Much of the data analysis herein is centered around a design condition of $M_\infty = 0.78$ and $C_{L,basic} = 0.44$. This design lift coefficient is based on the exposed wing panel and corresponds to an overall trimmed airplane lift coefficient of about 0.4, which is an average value for a representative mission.

The addition of winglets or a tip extension increases the optimum cruise lift coefficient for the airplane as a result of the rotation of the drag coefficient plotted against lift coefficient polar. Therefore, for a particular engine setting, the optimum cruise altitude would increase, while the thrust coefficient (or equivalent drag coefficient) would remain constant. Figure 10 shows the increase in lift coefficient for a constant drag coefficient resulting from the additional surfaces on the wind-tunnel model. These changes are equal to changes in the lift-drag ratio. As was stated in reference 1, the effects presented differ from those for a complete full-scale airplane. At full-scale conditions, the skin-friction-drag penalties associated with the additions would be somewhat less than those for the wind-tunnel test Reynolds number. More importantly, the

drag due to lift for the complete airplane would be greater than for the exposed panel of the wind-tunnel model. Therefore, the relative increase in lift coefficient for a constant drag coefficient would be less. It has been estimated that because of these two compensating factors the relative changes in lift-drag ratio for the complete full-scale airplane would be about 10 percent less than those presented in figure 10.

Upper winglet.- At low lift coefficients, the increase in wetted area due to the addition of the upper winglet results in additional skin-friction and form drag over the basic wing which is greater than the reduction in induced drag. The lift coefficient at which these two effects cancel is approximately 0.2 for cruise Mach numbers. For lift coefficients greater than 0.2, the reduction in induced drag predominates over the increases in skin-friction and form drag, and the drag-coefficient reduction increases as lift coefficient increases. Analysis of data indicates that for lift coefficients up to the design value, the reductions in induced drag over the basic wing due to the upper winglet are approximately 20 percent.

Figure 10 shows that the addition of the upper winglet results in an increase in lift-drag ratio of about 9 percent over the basic wing at cruise conditions. The increase in lift-drag ratio associated with the upper winglet tends to decrease with increasing lift coefficient. This effect is caused by wave drag and shock-induced boundary-layer separation at the wing-winglet juncture at higher lift coefficients.

Figure 7 shows that the addition of the upper winglet results in slightly more negative values of pitching-moment coefficient and also tends to reduce the longitudinal instability of the model (which is evident by a less positive slope of C_m versus C_L). The slope of the curve of lift coefficient plotted against angle of attack is slightly higher with the upper winglet added. The breaks in the curves of angle of attack and pitching-moment coefficient versus lift coefficient for the basic-wing and upper-winglet configurations occur at approximately the same lift coefficient ($C_L = 0.7$). The loss of lift on the upper-winglet configuration at higher lift coefficients (see figs. 7(b) to 7(d)) is caused by increased boundary-layer separation on the wing, which tends to unload the outboard portion of the wing.

Upper and lower winglets.- Figure 6 shows that at cruise Mach numbers, the addition of the lower winglet has little effect relative to the upper-winglet configuration on the variation of drag coefficient with lift coefficient at lift coefficients of 0.6 to 0.7. At higher lift coefficients the favorable influence of the lower winglet on the upper winglet retards separation on the upper winglet by decreasing the local angle of attack, particularly over the root regions, and by lowering the leading-edge pressure peak. (See ref. 4.) Thus, the favorable effects shown by the upper winglet of reducing the induced drag and increasing the total lift continue beyond lift coefficients of 0.7. The breaks in the curves of angle of attack and pitching-moment coefficient plotted against lift coefficient are more gradual than with the upper winglet alone. (See fig. 7.)

Figure 8 shows the boundary-layer visualization photographs for the configuration with upper and lower winglets at $M_\infty = 0.78$ and $C_L \approx 0.48$. Cellophane tape was placed over the rows of surface pressure orifices on the wing and wing-

let to prevent oil from entering these orifices. The edges of the tape resulted in chordwise stripes in the photographs. Seepage of oil under the tape near the leading edge and along the transition strip resulted in bright spots on the photographs. The winglets produce no adverse boundary-layer flow for cruise conditions. Photographs (not presented) for the same lift coefficient at a slightly higher Mach number (0.80) also show no adverse flow characteristics of the boundary layer.

Tip extension.- Analysis of figure 6 shows that the wing-tip extension provides approximately a 10-percent reduction in induced drag over the basic wing for lift coefficients up to the design condition. Figure 10 shows that the tip extension produces an increase in lift-drag ratio of about 4 percent over the basic wing at cruise conditions. This is approximately half of the increase associated with the winglet configurations.

The breaks in the variations of angle of attack and pitching-moment coefficient with lift coefficient (fig. 7) also occur at a lift coefficient of 0.70, and the slopes of both curves after the break are approximately the same as the slopes for the upper-and-lower-winglet and basic-wing configurations. As with both winglet configurations, the additional lifting surface behind the moment center of the airplane results in slightly less longitudinal aerodynamic instability than with the basic wing. This effect is shown in figure 7 as a slightly less positive slope in the pitching-moment coefficient plotted against lift coefficient. The increment in pitching-moment coefficient due to the tip extension is more than twice that for the upper-winglet configuration; therefore, the tip extension would have an additional small trim drag penalty relative to the upper winglet.

Bending moments.- Winglets and tip extensions result in somewhat higher bending moments at the wing root. An important trade-off must be considered between the benefits of increased aerodynamic efficiency and the weight penalties associated with the heavier wing structure required to handle the increased bending moments. Consequently, comparisons of the different wing-tip configurations must be made on the basis of equal bending-moment increments on the wing structure. Generally, the wing structural design is governed by the bending moments at the higher lift coefficients associated with a higher than 1g load condition.

Figure 9 shows the variations with lift coefficient of incremental bending-moment coefficients at the wing-fuselage juncture for Mach numbers of 0.70 and 0.78. The bending-moment coefficients presented were computed in two steps. First, the rolling moments measured at the balance center were transferred to the wing-fuselage juncture. Then the bending moments due to winglet side force were added to the rolling moments. These bending moments were calculated by multiplying the side-force increments of the winglets (from integrations of the pressure distributions of ref. 4) times the vertical distance from the moment reference center to the elastic axis of the wing root. The bending moments associated with side forces on the wing panel (due to wing dihedral) were not computed. These bending moments are nearly equal for all the configurations at the same lift coefficient. Inclusion of these bending-moment increments would reduce the absolute values presented in figure 9 slightly; however, the relative increments between configurations would remain constant.

The bending-moment-coefficient increments at the design lift coefficient of 0.44 are increased approximately 3 to 4 percent relative to the basic wing. At lift coefficients higher than 0.5, the upper-winglet configuration shows decreasing bending-moment-coefficient increments, while the increments for the tip extension tend to increase. The addition of the lower winglet causes an increase in the bending-moment-coefficient increment, but it is still less than the tip-extension increment at $M_\infty = 0.70$ and approximately equal at $M_\infty = 0.78$. (Bending-moment-coefficient increments are not presented at lift coefficients greater than 0.70 at $M_\infty = 0.78$ because the wing is stalled (fig. 7(c)) and therefore the data are strongly dependent on Reynolds number.)

The reason for these trends is that as the wing lift coefficient increases to the higher values, the normal-force coefficients on the winglets do not increase as rapidly as do the section lift coefficients of the tip extension. (See ref. 4.)

Wing-tip vortex.- The flow-field cross-flow velocity vectors measured 2 wing-tip chords downstream of the wing tip are presented in figure 11 for two cruise Mach numbers. The flow pattern behind the basic wing (figs. 11(a) and 11(c)) suggests a typical wing-tip vortex circulation. The center of the rake is positioned approximately at the vortex core. The addition of the upper winglet (figs. 11(b) and 11(d)) substantially reduces the magnitude of the velocity vectors in the vortex-core region and disrupts the whole vortex to the point where a core is not discernible at this distance downstream.

Reductions in induced drag of the wing are directly related to reduction of the total energy of the circulation. The reductions in induced drag produced by the upper winglet are evident primarily by the reductions in the kinetic energy of the vortex core, which is proportional to the cross-flow velocity squared. Unpublished far-field data from the Langley vortex research facility confirm that the winglets delay formation of the vortex and that the velocities in the core region of the vortex are reduced by an increment proportional to the reductions in induced drag for those configurations.

Second-Segment Climb

Variations of incremental drag coefficient with lift coefficient are presented in figure 14 for the configurations with trailing-edge flaps. These increments are also equivalent to increments in the lift-drag ratio. Incremental drag is presented for $M_\infty = 0.30$ rather than incremental lift which was presented for cruise Mach numbers, because airplanes cannot be flown with the same flexibility in lift coefficient during second-segment climb as is possible during cruise. Data were not obtained for all possible combinations of wing-tip and leading- and trailing-edge-flap configurations.

No flaps.- Data for the configuration without flaps are shown in figures 12(a) and 13(a). The upper-and-lower-winglet configuration shows a benefit over the basic wing in aerodynamic efficiency and has decreased longitudinal instability at lift coefficients up to 0.9, after which the wing initially stalls.

Trailing-edge flaps.- Data for the configurations with trailing-edge flaps added are shown in figures 12(b) and 13(b). These data are representative of first-generation jet transports similar to the KC-135A. The trailing-edge flaps delay stall on the wing to a lift coefficient of 1.1. The addition of the upper winglet produces reductions in total drag coefficient of up to 11 percent at a lift coefficient just prior to stall. This is equivalent to a 0.0085 reduction in drag coefficient. Figure 14 shows that at a lift coefficient near 1.0, the upper winglet produces an increase in lift-drag ratio of approximately 10 percent.

Again, slight decreases in longitudinal instability are shown (fig. 13(b)) by a less positive slope of pitching-moment coefficient plotted against lift coefficient. The upper-winglet configuration results in more negative values of C_m and also shows a slightly greater tendency to pitch up after stall.

The addition of the upper and lower winglets produces reductions in drag coefficient less than the upper winglet only, or about 10 percent (0.0077) near stall conditions, and produces an increase in lift-drag ratio of about 9 percent at a lift coefficient of 1.0 (fig. 14). The upper-and-lower-winglet configuration shows lift and pitching-moment trends similar to the upper-winglet configuration.

At cruise Mach numbers, the lower winglet has been shown to reduce the leading-edge pressure peak of the upper winglet and thereby extend aerodynamic effectiveness to lift coefficients higher than for the upper winglet alone. At a Mach number of 0.30, the lower winglet experiences relatively high drag coefficients due to high loading and some flow separation on this surface.

The addition of the tip extension results in drag coefficients which are 2 to 3 percent higher than those for the upper-winglet configuration. At a lift coefficient of 1.0, the tip extension produces an increase in lift-drag ratio of approximately 6.5 percent. The tip-extension configuration also exhibits a slightly higher lift coefficient and a more negative pitching-moment increment than does the upper-winglet configuration. Therefore, the trim drag penalty associated with the pitching-moment increments would be higher for the tip extension than for the upper winglet.

Leading- and trailing-edge flaps.- Data for configurations with leading- and trailing-edge flaps are presented in figures 12(c) and 13(c). These configurations are designed to simulate the effects of winglets on the second-segment-climb characteristics of most present jet transports. The addition of the leading-edge flap moves the point at which the wing initially stalls to a lift coefficient of 1.3. The upper-winglet configuration produces reductions in drag coefficient of up to 9 percent at the stall lift coefficient. Again, the upper-winglet configuration is slightly less unstable longitudinally than the basic wing.

As for the configurations with only trailing-edge flaps, addition of the lower winglet results in slightly higher values of drag coefficient below the stall lift coefficient. The upper-and-lower-winglet configuration also produces a slightly higher lift coefficient and a more negative pitching-moment coefficient than the upper-winglet configuration.

SUMMARY OF RESULTS

A wind-tunnel investigation of winglets mounted on the tip of a 0.07-scale KC-135A jet transport model wing has been conducted. Configurations with an upper winglet only and with upper and lower winglets are compared with a simple wing-tip extension which is designed to produce the same increase in bending moment at the wing root (at a 1g load factor) as do the winglets. Data are presented at four high subsonic Mach numbers and one low subsonic Mach number, and indicate the following conclusions:

1. Both winglet configurations reduce induced drag by approximately 20 percent at design cruise conditions. The tip extension reduces induced drag by about 10 percent at design conditions.

2. At cruise conditions winglets produce improvements in lift-drag ratio of about 9 percent. At the same conditions the tip extension produces a 4-percent improvement in lift-drag ratio.

3. The negative increments in pitching-moment coefficient due to the winglets are less than those produced by the tip extension.

4. All the wing-tip configurations investigated produce an increment in wing root bending moment of approximately 3 to 4 percent for lift coefficients up to the design value at Mach numbers of 0.70 and 0.78. At lift coefficients significantly higher than the cruise values, the bending increments for the tip extension increase, while those for the upper winglet tend to decrease.

5. Both winglet configurations produce reductions in induced drag greater than those produced by the tip extension at second-segment-climb conditions with trailing-edge flaps. The upper-winglet, upper-and-lower-winglet, and tip-extension configurations produce increases in lift-drag ratio (at a lift coefficient of 1.0) of 10 percent, 9 percent, and 6.5 percent, respectively, with trailing-edge flaps.

6. The winglets delay the formation of the wing-tip vortex and lessen the cross-flow velocity vectors in the core area.

Langley Research Center
National Aeronautics and Space Administration
Hampton, VA 23665
April 18, 1977

REFERENCES

1. Whitcomb, Richard T.: A Design Approach and Selected Wind-Tunnel Results at High Subsonic Speeds for Wing-Tip Mounted Winglets. NASA TN D-8260, 1976.

2. Flechner, Stuart G.; Jacobs, Peter F.; and Whitcomb, Richard T.: A High Subsonic Speed Wind-Tunnel Investigation of Winglets on a Representative Second-Generation Jet Transport Wing. NASA TN D-8264, 1976.

3. Jacobs, Peter F.; and Flechner, Stuart G.: The Effect of Winglets on the Static Aerodynamic Stability Characteristics of a Representative Second Generation Jet Transport Model. NASA TN D-8267, 1976.

4. Montoya, Lawrence C.; Flechner, Stuart G.; and Jacobs, Peter F.: Effect of Winglets on a First-Generation Jet Transport Wing. II - Pressure and Spanwise Load Distributions for a Semispan Model at High Subsonic Speeds. NASA TN D-8474, 1977.

5. Montoya, Lawrence C.; Jacobs, Peter F.; and Flechner, Stuart G.: Effect of Winglets on a First-Generation Jet Transport Wing. III - Pressure and Spanwise Load Distributions for a Semispan Model at Mach 0.30. NASA TN D-8478,1977.

6. Mechtly, E. A.: The International System of Units - Physical Constants and Conversion Factors (Second Revision). NASA SP-7012, 1973.

7. Schaefer, William T., Jr.: Characteristics of Major Active Wind Tunnels at the Langley Research Center. NASA TM X-1130, 1965.

8. Braslow, Albert L.; and Knox, Eugene C.: Simplified Method for Determination of Critical Height of Distributed Roughness Particles for Boundary-Layer Transition at Mach Numbers From 0 to 5. NACA TN 4363, 1958.

9. Blackwell, James A., Jr.: Preliminary Study of Effects of Reynolds Number and Boundary-Layer Transition Location on Shock-Induced Separation. NASA TN D-5003, 1969.

10. Loving, Donald L.; and Katzoff, Samuel: The Fluorescent-Oil Film Method and Other Techniques for Boundary-Layer Flow Visualization. NASA MEMO 3-17-59L, 1959.

11. Patterson, James C., Jr.; and Flechner, Stuart G.: An Exploratory Wind-Tunnel Investigation of the Wake Effect of a Panel Tip-Mounted Fan-Jet Engine on the Lift-Induced Vortex. NASA TN D-5729, 1970.

12. Brooks, Joseph D.: Some Anomalies Observed in Wind-Tunnel Tests of a Blunt Body at Transonic and Supersonic Speeds. NASA TN D-8237, 1976.

TABLE I.- AIRFOIL COORDINATES FOR WINGLETS

x/c	z/c for -	
	Upper surface	Lower surface
0	0	0
.0020	.0077	-.0032
.0050	.0119	-.0041
.0125	.0179	-.0060
.0250	.0249	-.0077
.0375	.0296	-.0090
.0500	.0333	-.0100
.0750	.0389	-.0118
.1000	.0433	-.0132
.1250	.0469	-.0144
.1500	.0499	-.0154
.1750	.0525	-.0161
.2000	.0547	-.0167
.2500	.0581	-.0175
.3000	.0605	-.0176
.3500	.0621	-.0174
.4000	.0628	-.0168
.4500	.0627	-.0158
.5000	.0618	-.0144
.5500	.0599	-.0122
.5750	.0587	-.0106
.6000	.0572	-.0090
.6250	.0554	-.0071
.6500	.0533	-.0052
.6750	.0508	-.0033
.7000	.0481	-.0015
.7250	.0451	.0004
.7500	.0419	.0020
.7750	.0384	.0036
.8000	.0349	.0049
.8250	.0311	.0060
.8500	.0270	.0065
.8750	.0228	.0064
.9000	.0184	.0059
.9250	.0138	.0045
.9500	.0089	.0021
.9750	.0038	-.0013
1.0000	-.0020	-.0067

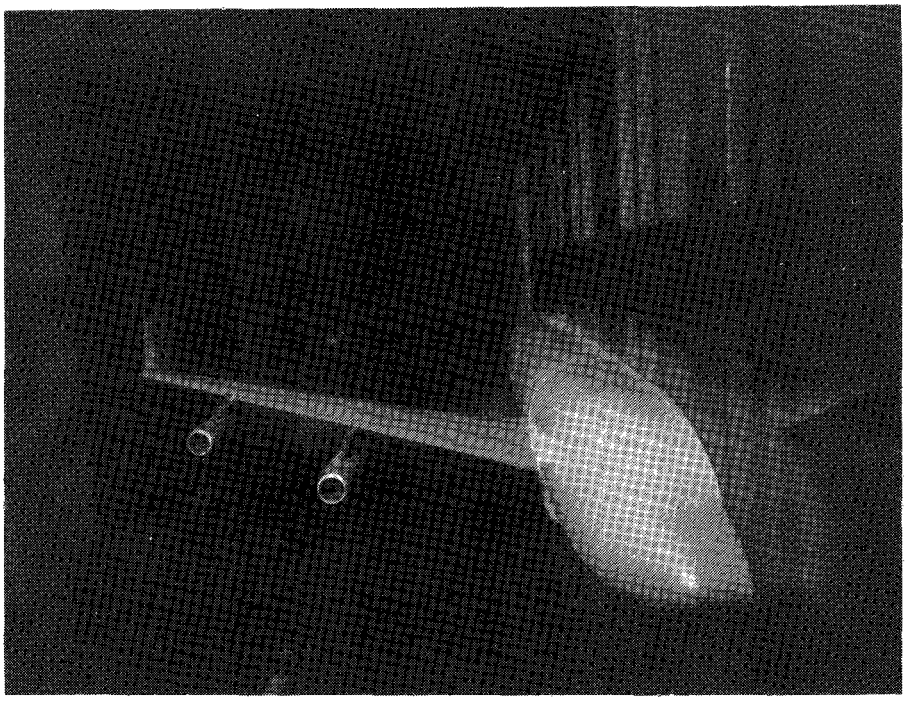

L-75-8430

(a) Complete configuration.

L-75-8429

(b) Winglets.

Figure 1.- Wind-tunnel model.

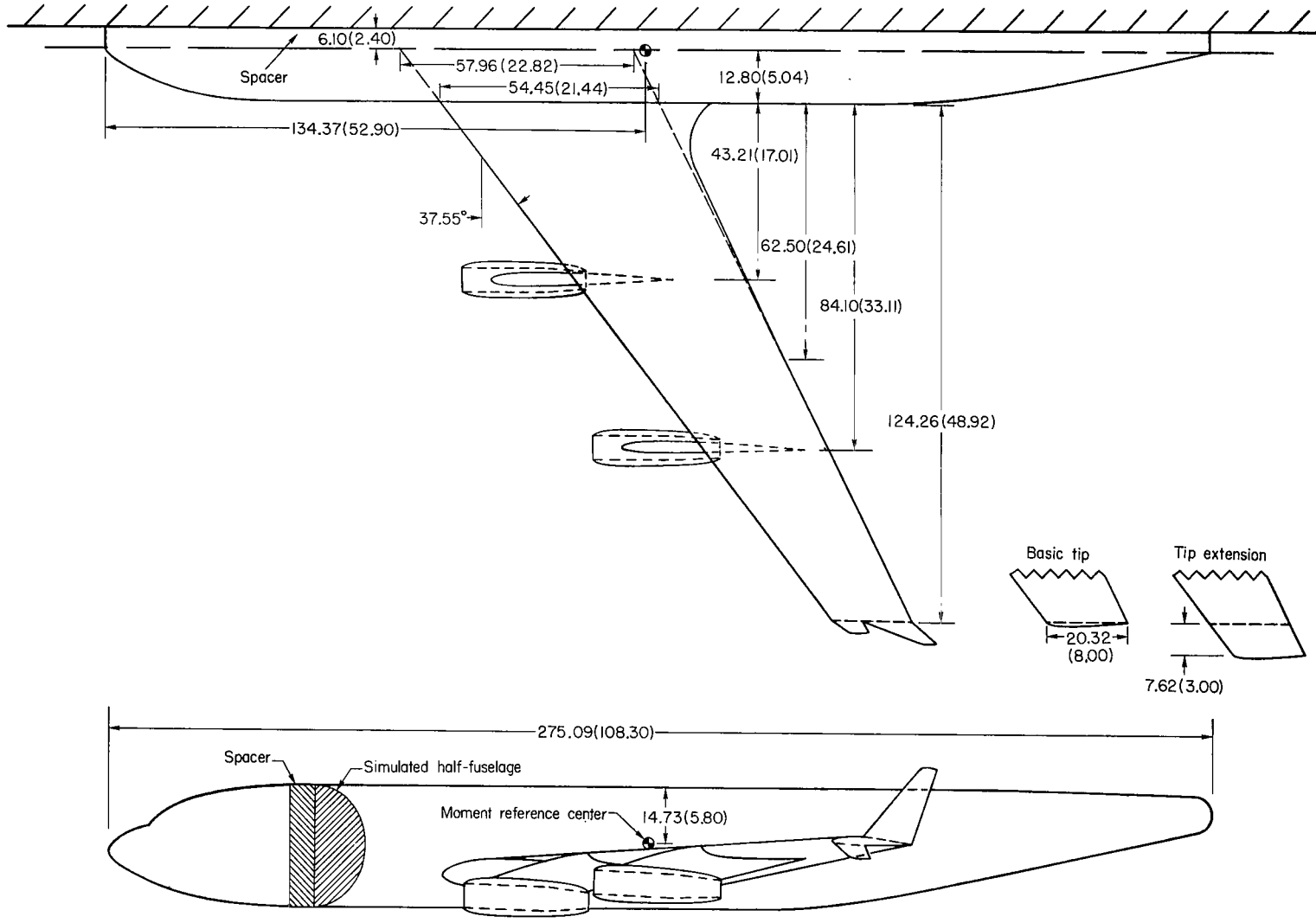

(a) General layout of model.

Figure 2.- Drawings of semispan model. Dimensions in centimeters (inches).

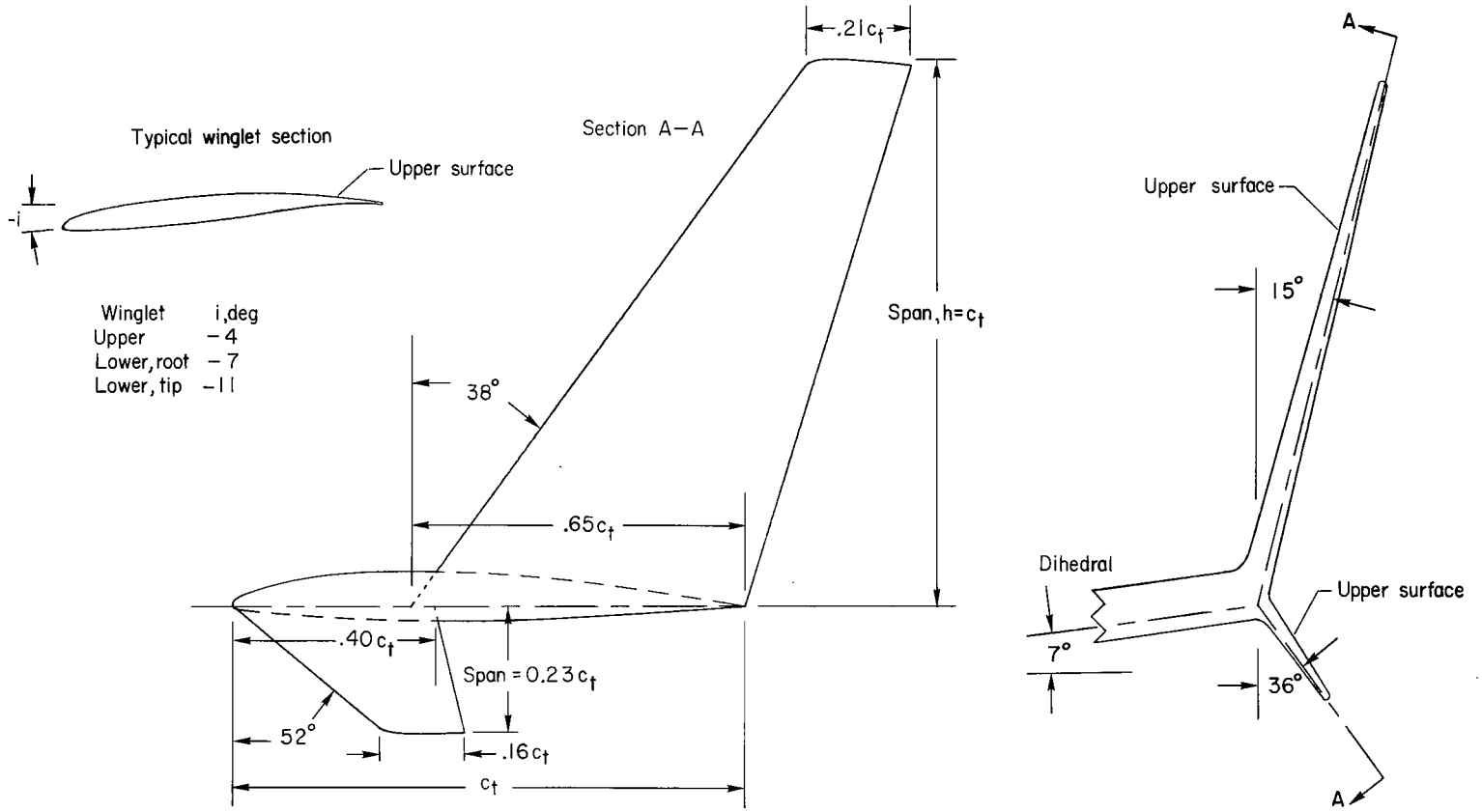

(b) Winglet details.

Figure 2.- Concluded.

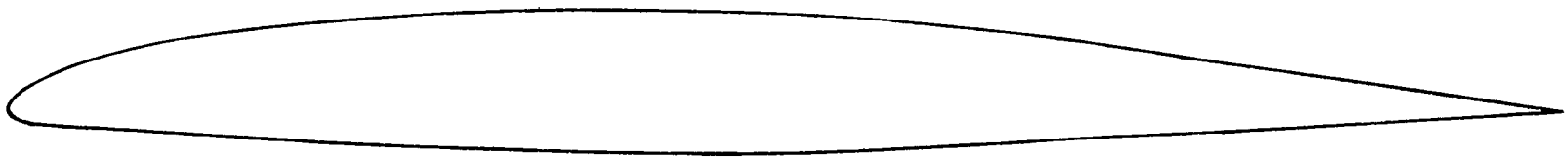

Figure 3.- Typical outboard wing airfoil section.

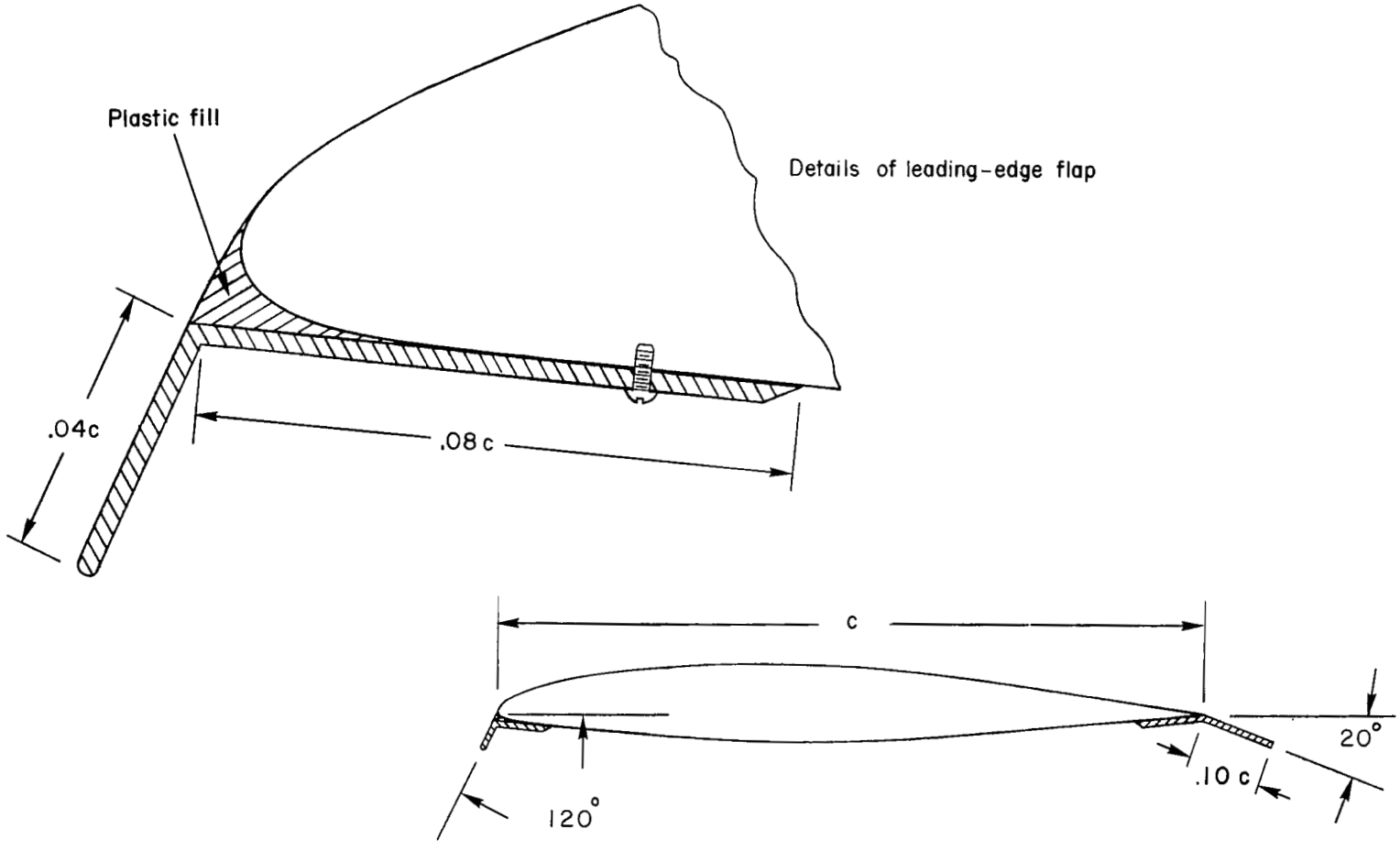

(a) Flap details.

Figure 4.- Drawings of leading- and trailing-edge flaps.

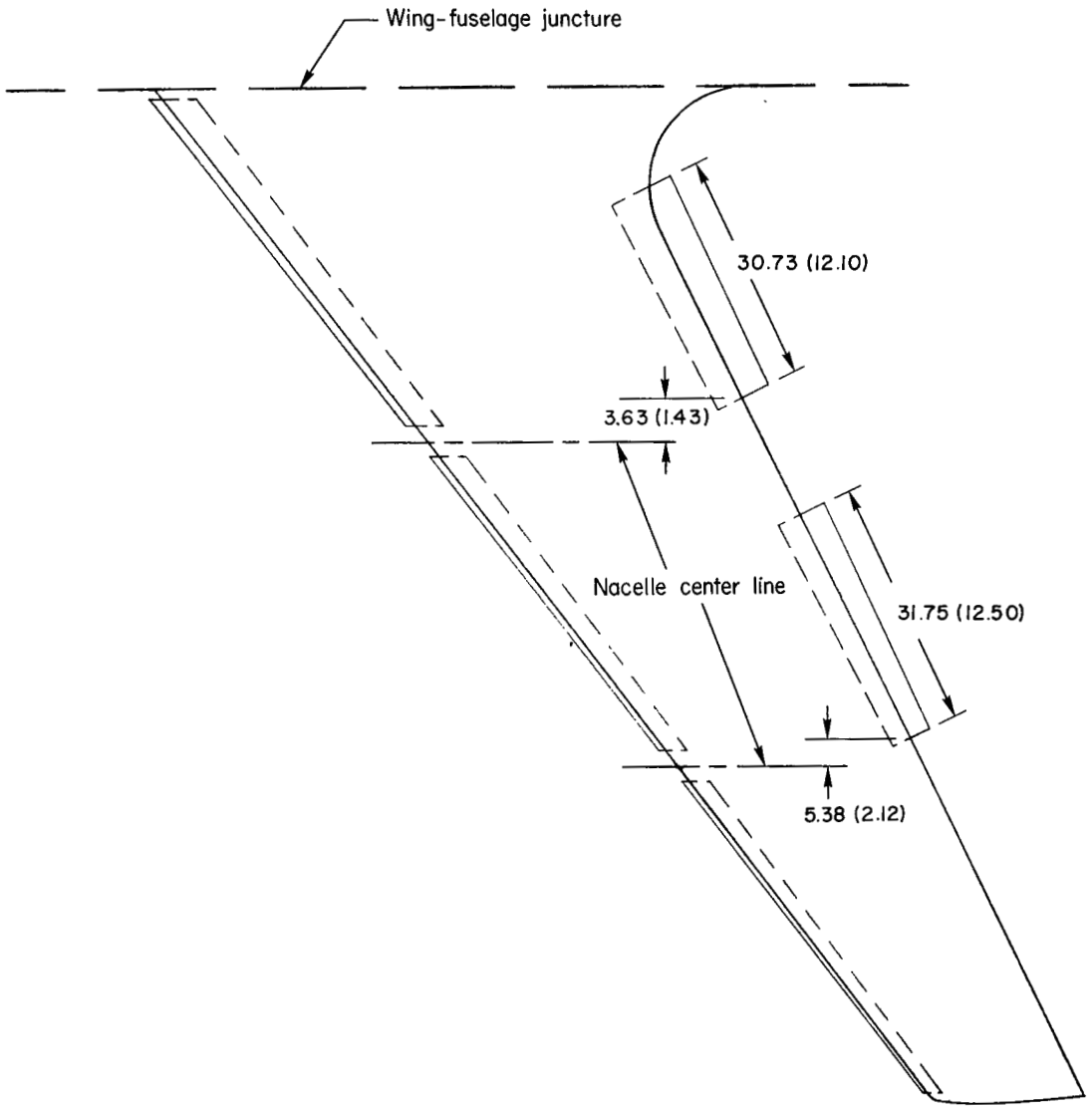

(b) Flap locations. Dimensions are in centimeters (inches).

Figure 4.- Concluded.

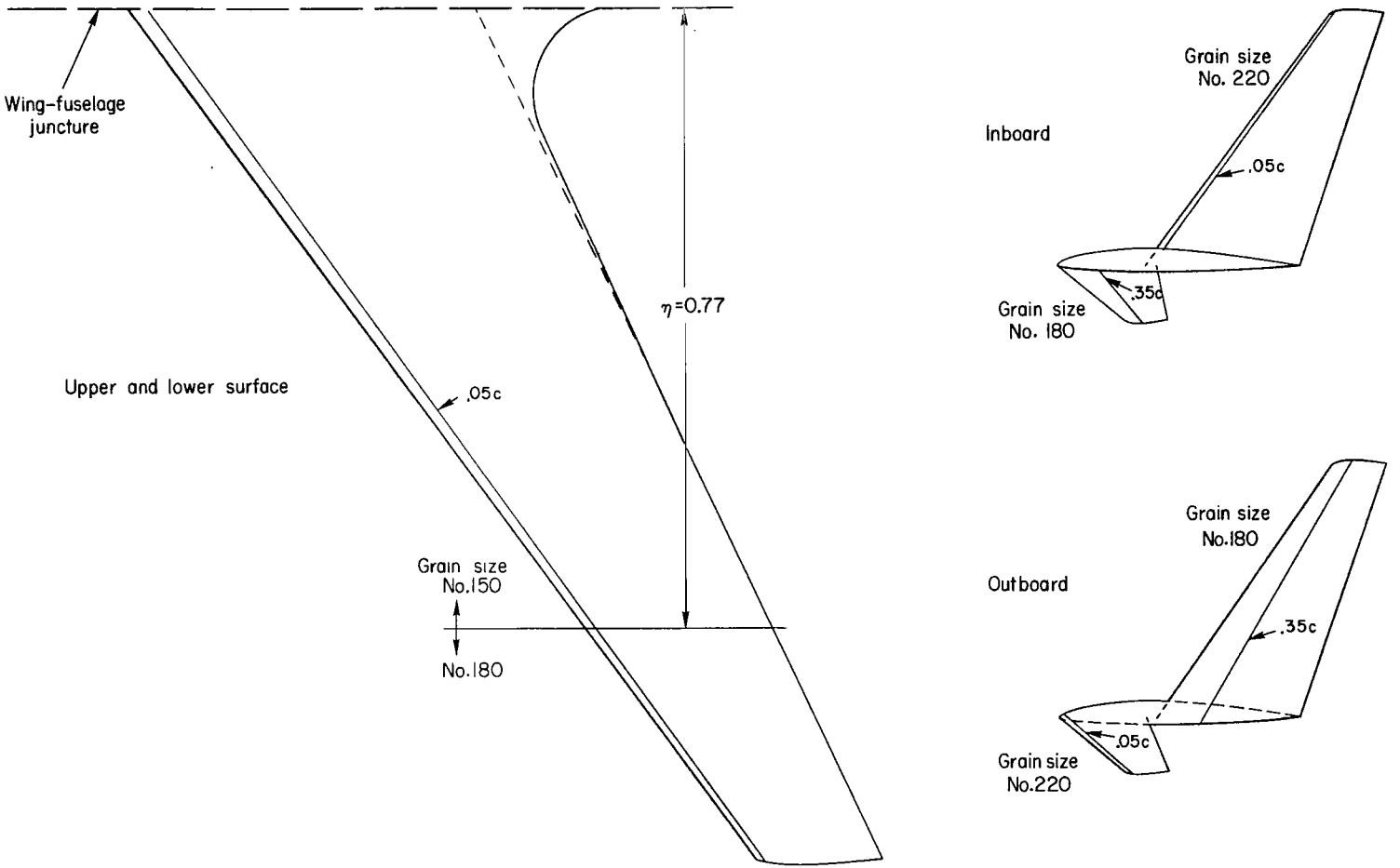

Figure 5.- Location of boundary-layer transition strips.

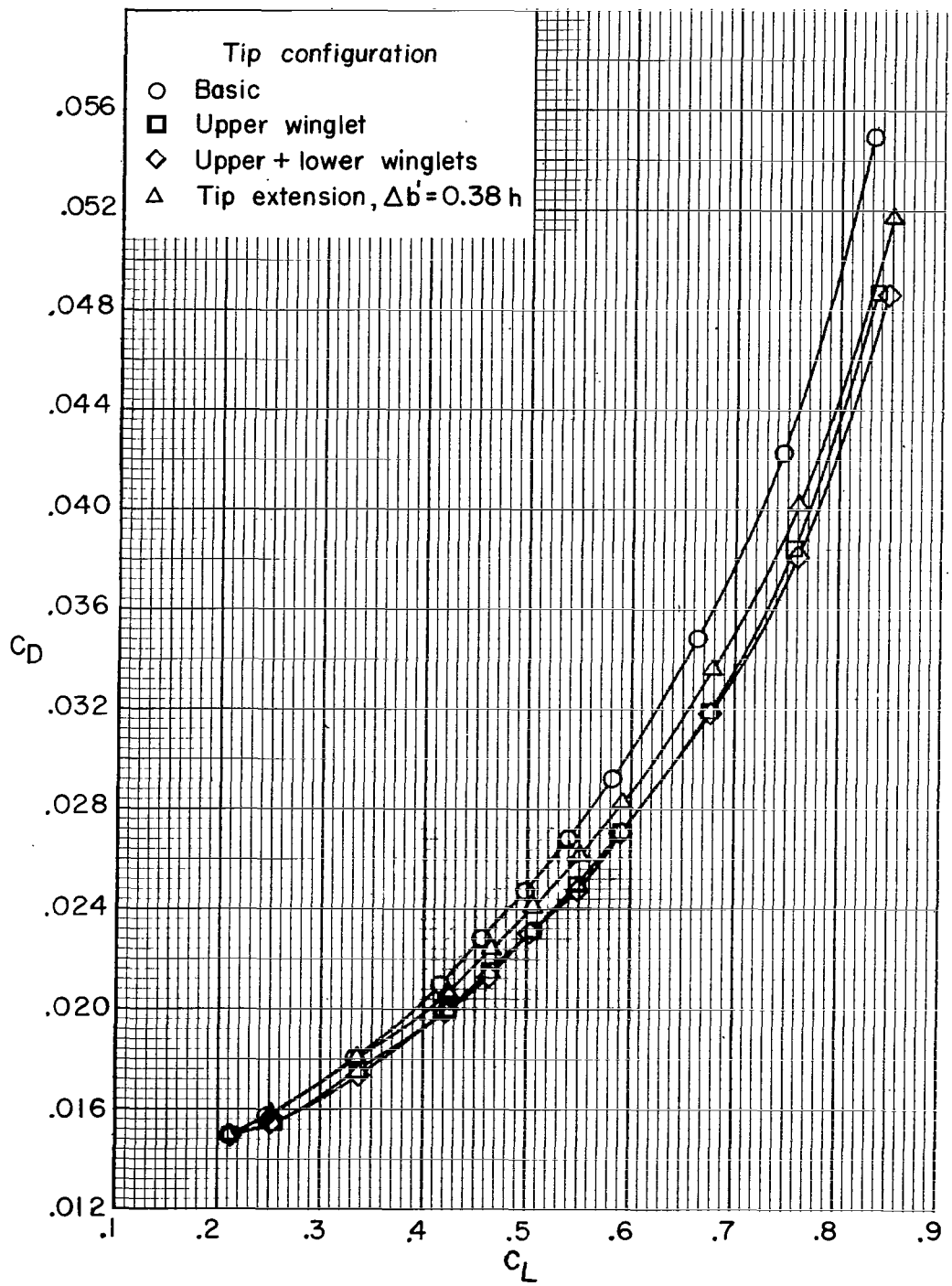

(a) $M_\infty = 0.70$.

Figure 6.- Variation of drag coefficient with lift coefficient.

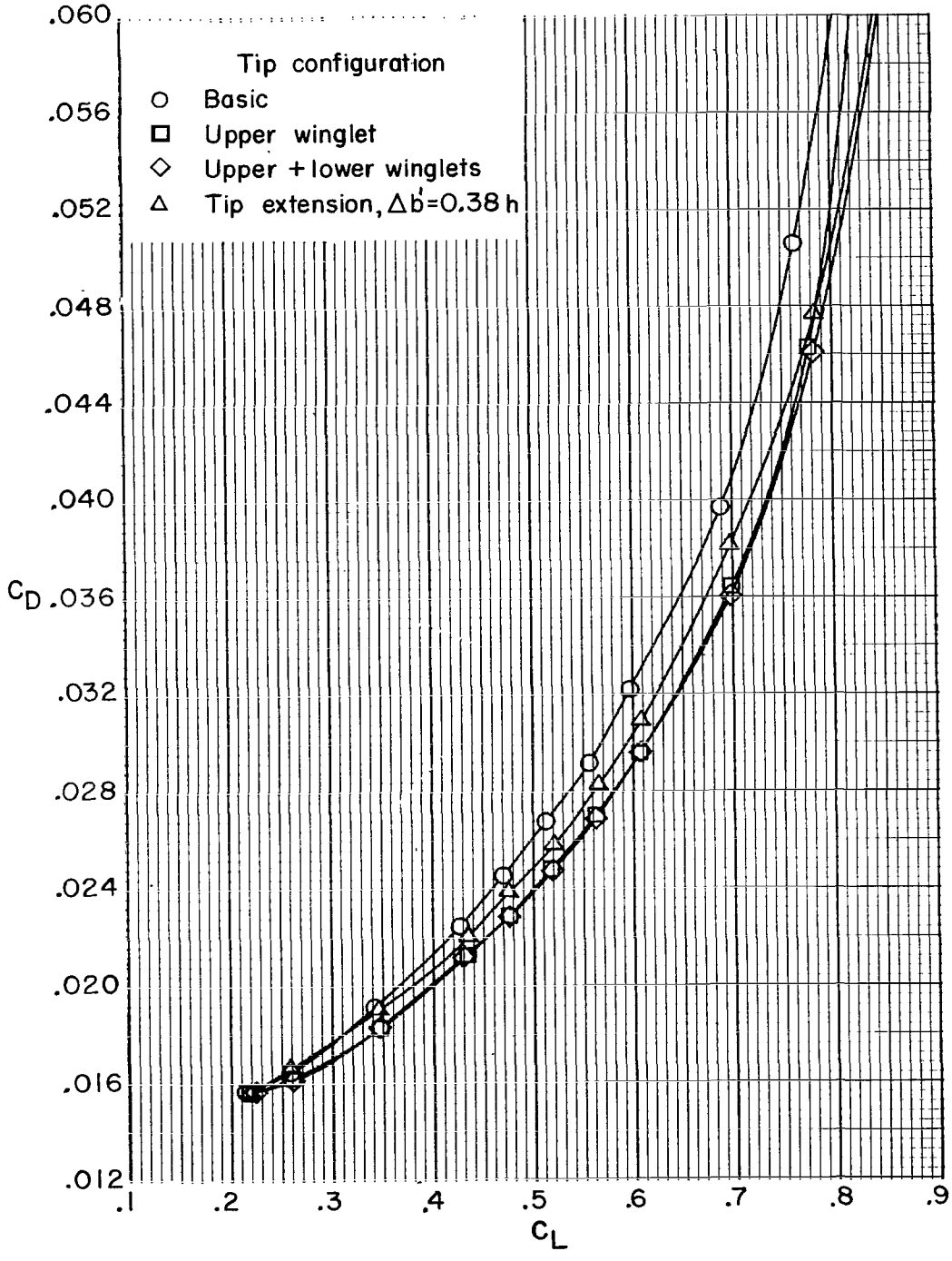

(b) $M_\infty = 0.75$.

Figure 6.- Continued.

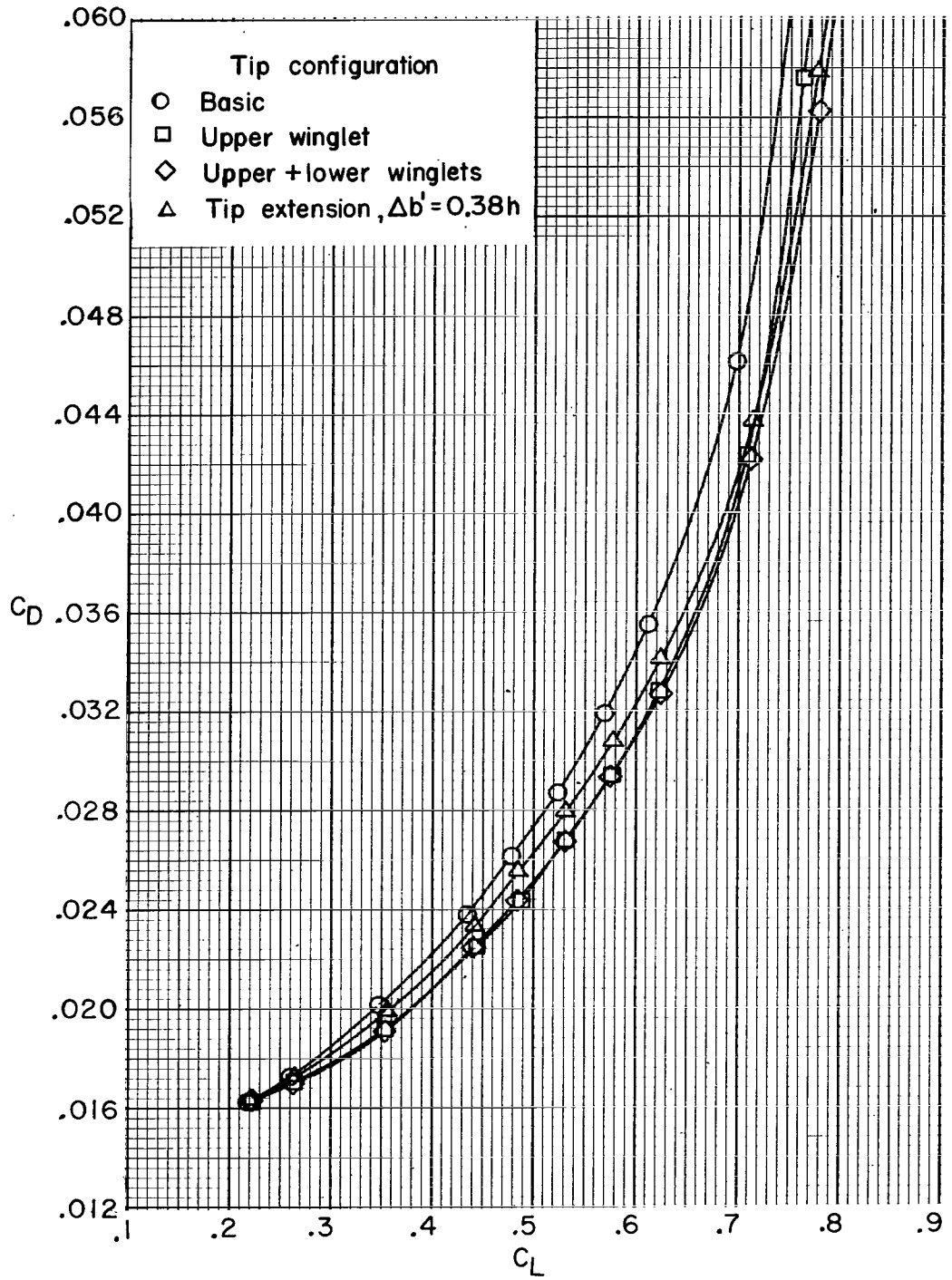

(c) $M_\infty = 0.78$.

Figure 6.- Continued.

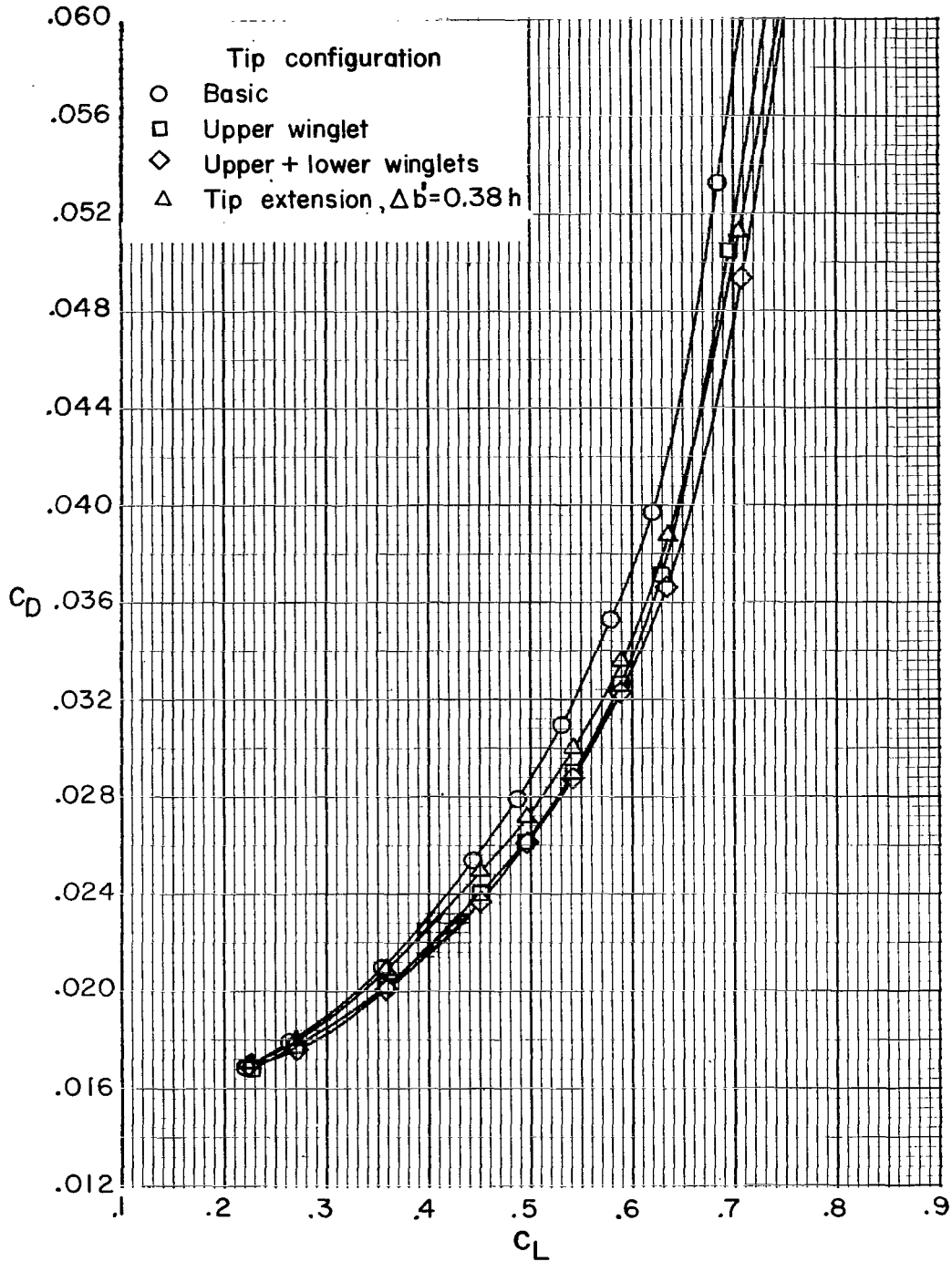

(d) $M_\infty = 0.80$.

Figure 6.- Concluded.

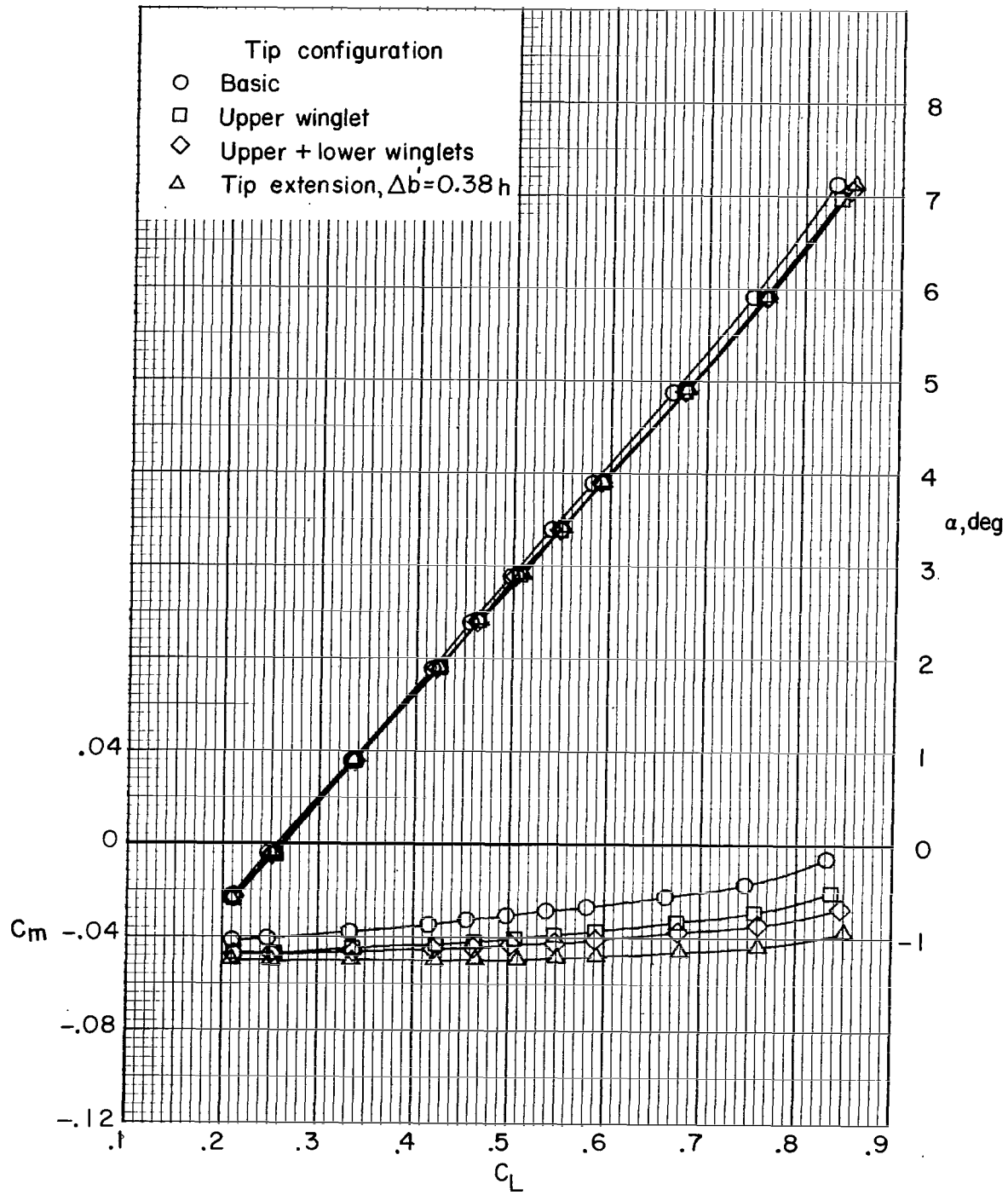

(a) $M_\infty = 0.70$.

Figure 7.- Variations of pitching-moment coefficient and angle of attack with lift coefficient.

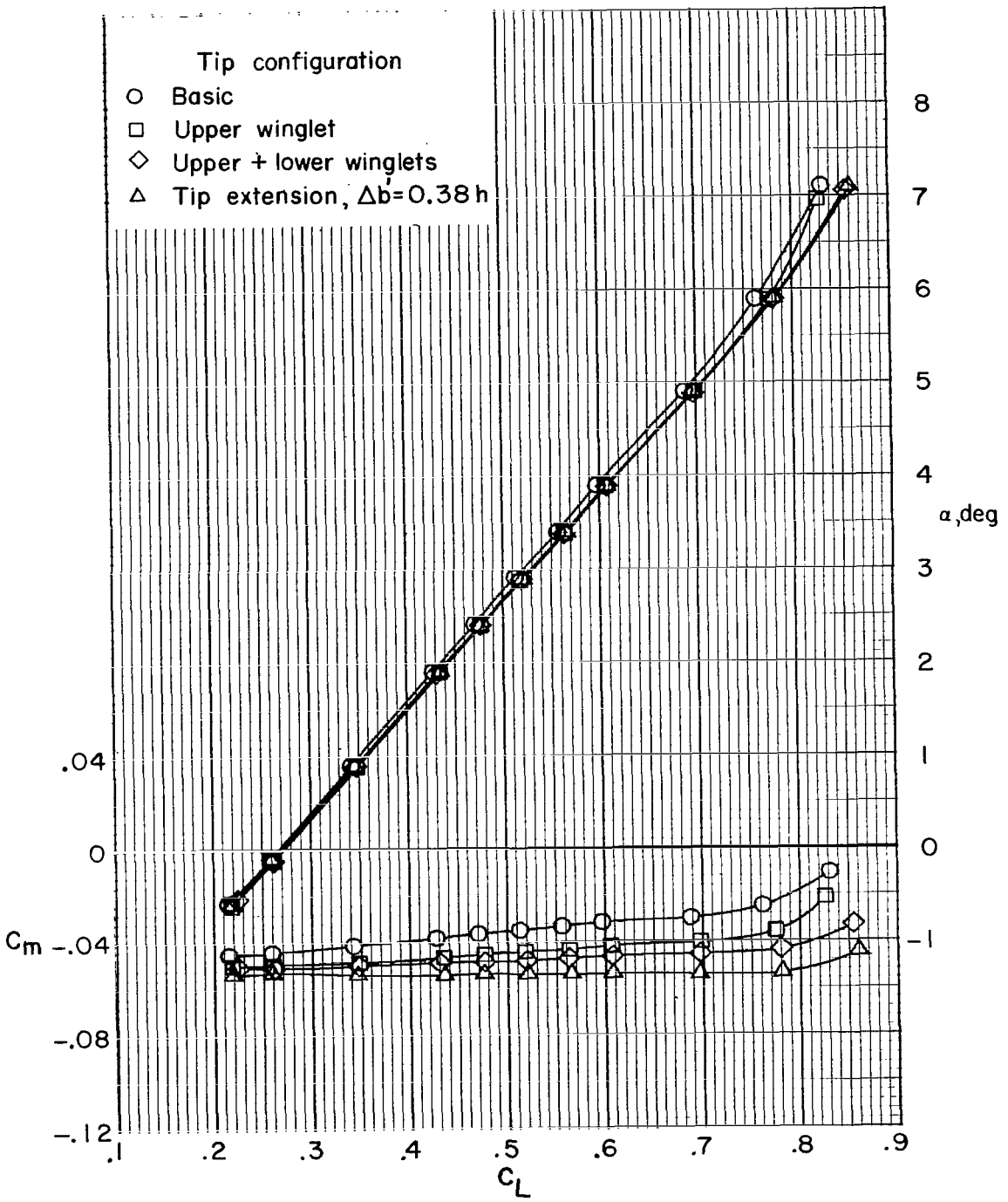

(b) $M_\infty = 0.75$.

Figure 7.- Continued.

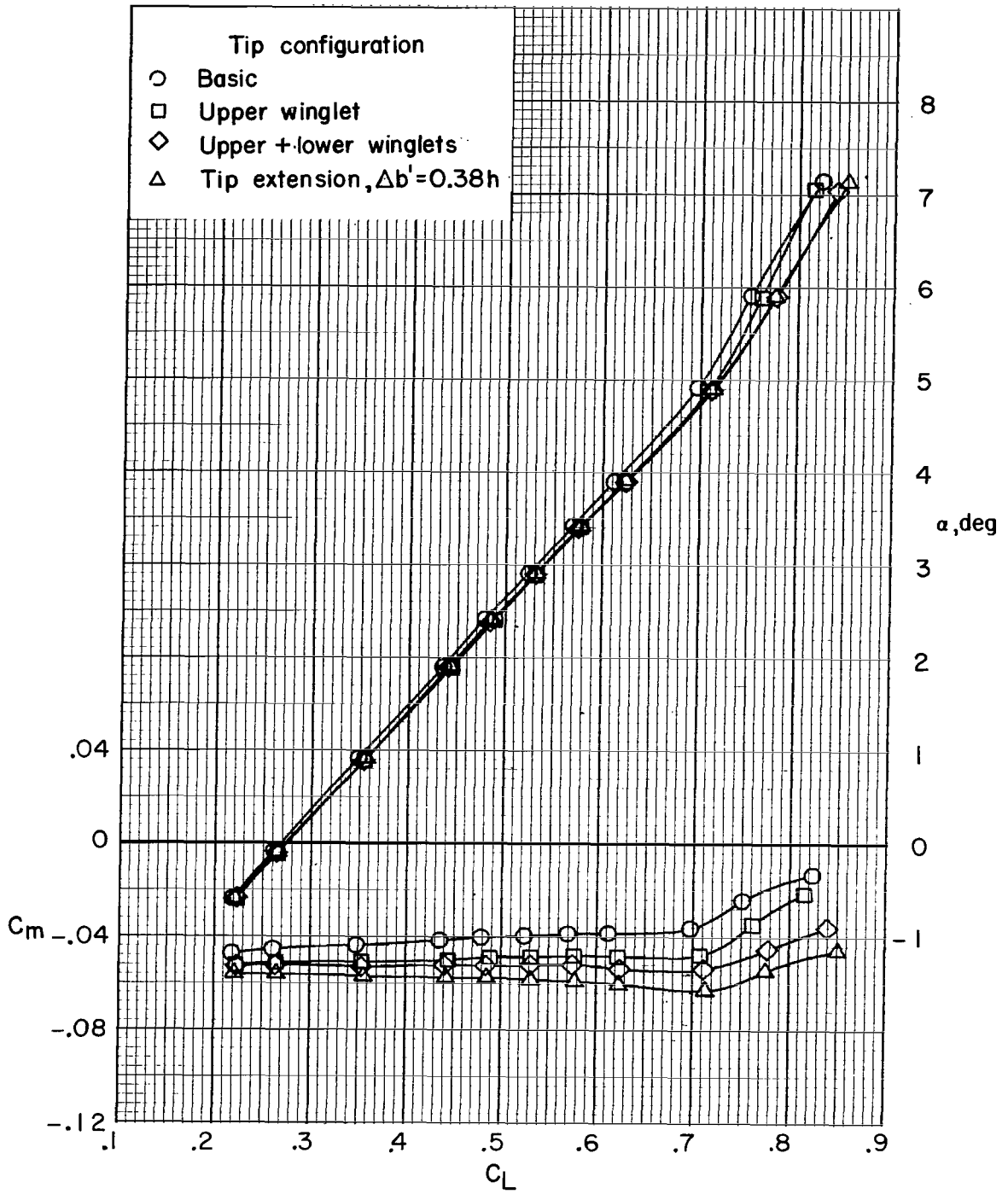

(c) $M_\infty = 0.78$.

Figure 7.- Continued.

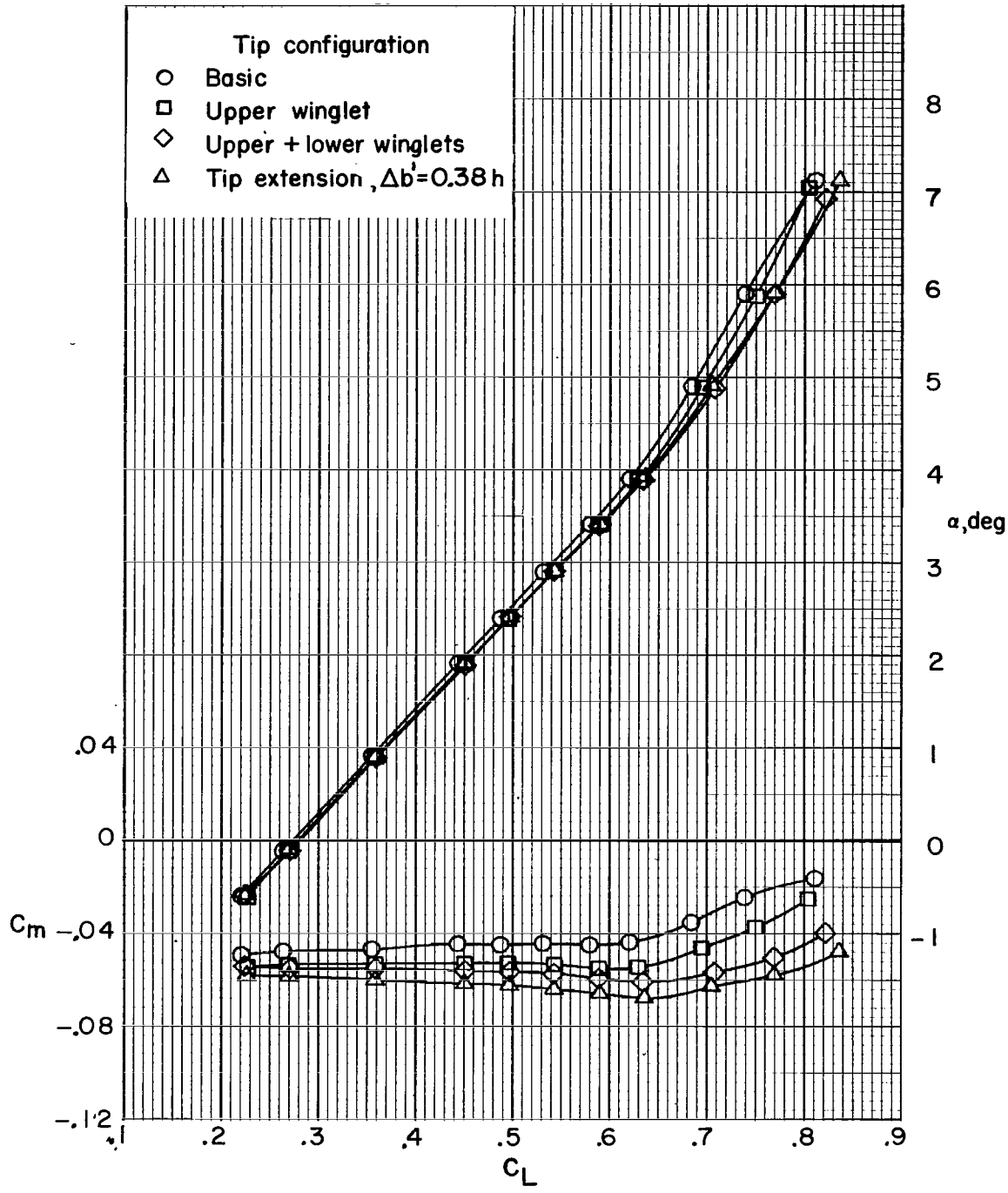

(d) $M_\infty = 0.80$.

Figure 7.- Concluded.

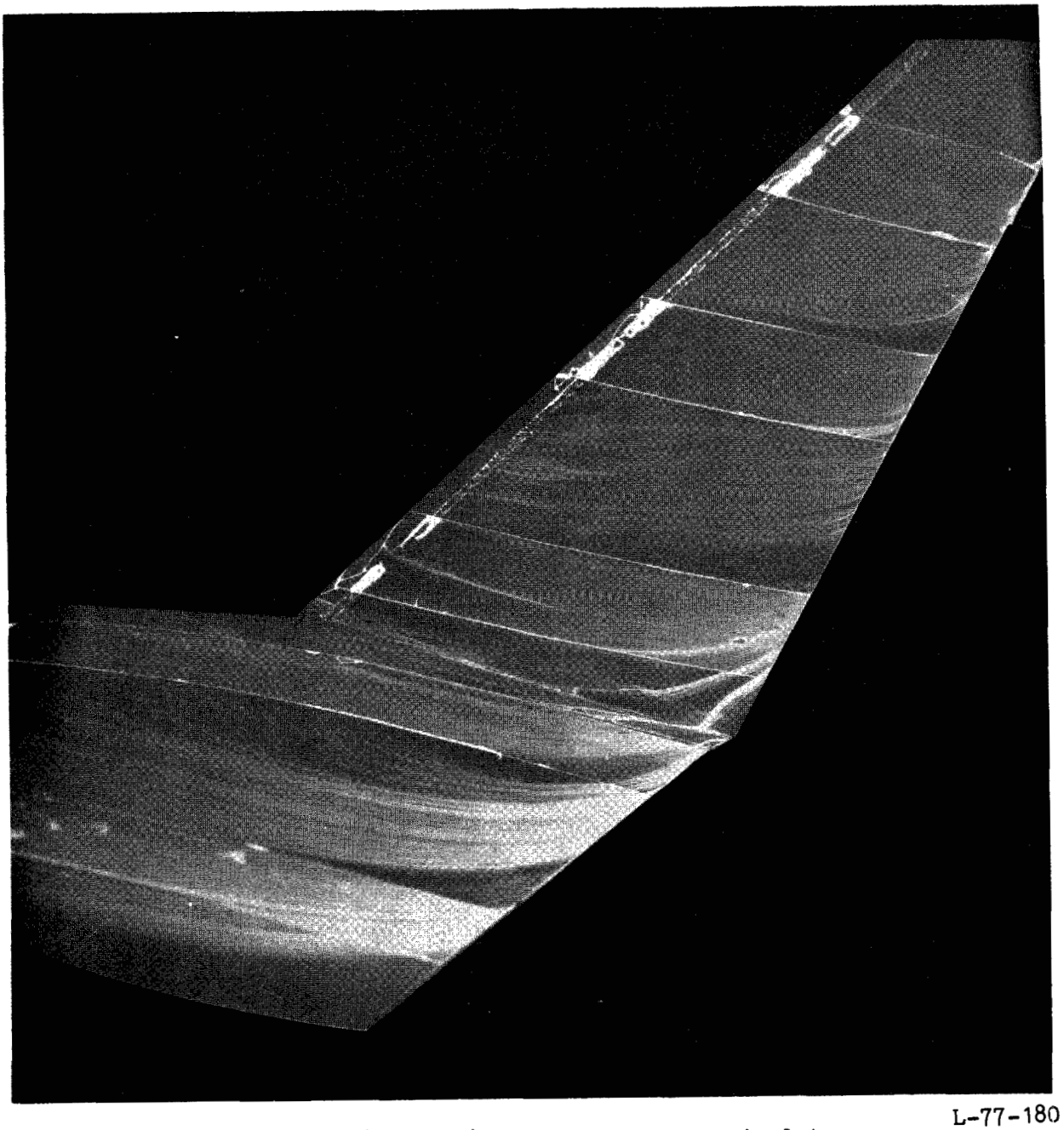

L-77-180

(a) Upper (inboard) surface of upper winglet.

Figure 8.- Fluorescent-oil-film flow-visualization photographs (upper and lower winglets). $M_\infty = 0.78$; $C_L = 0.48$.

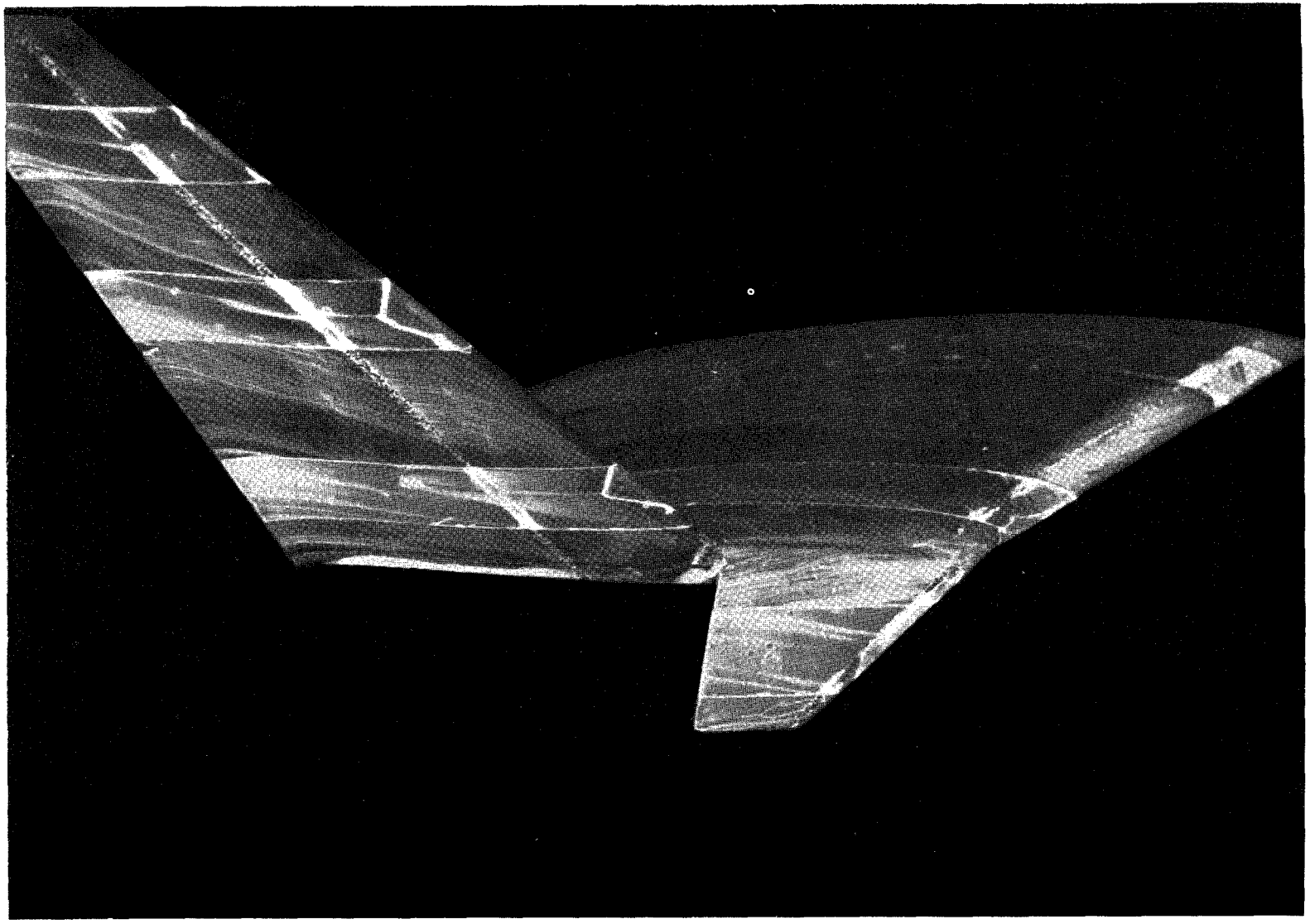

L-77-181

(b) Lower (outboard) surface of upper winglet and upper (outboard) surface of lower winglet.

Figure 8.- Concluded.

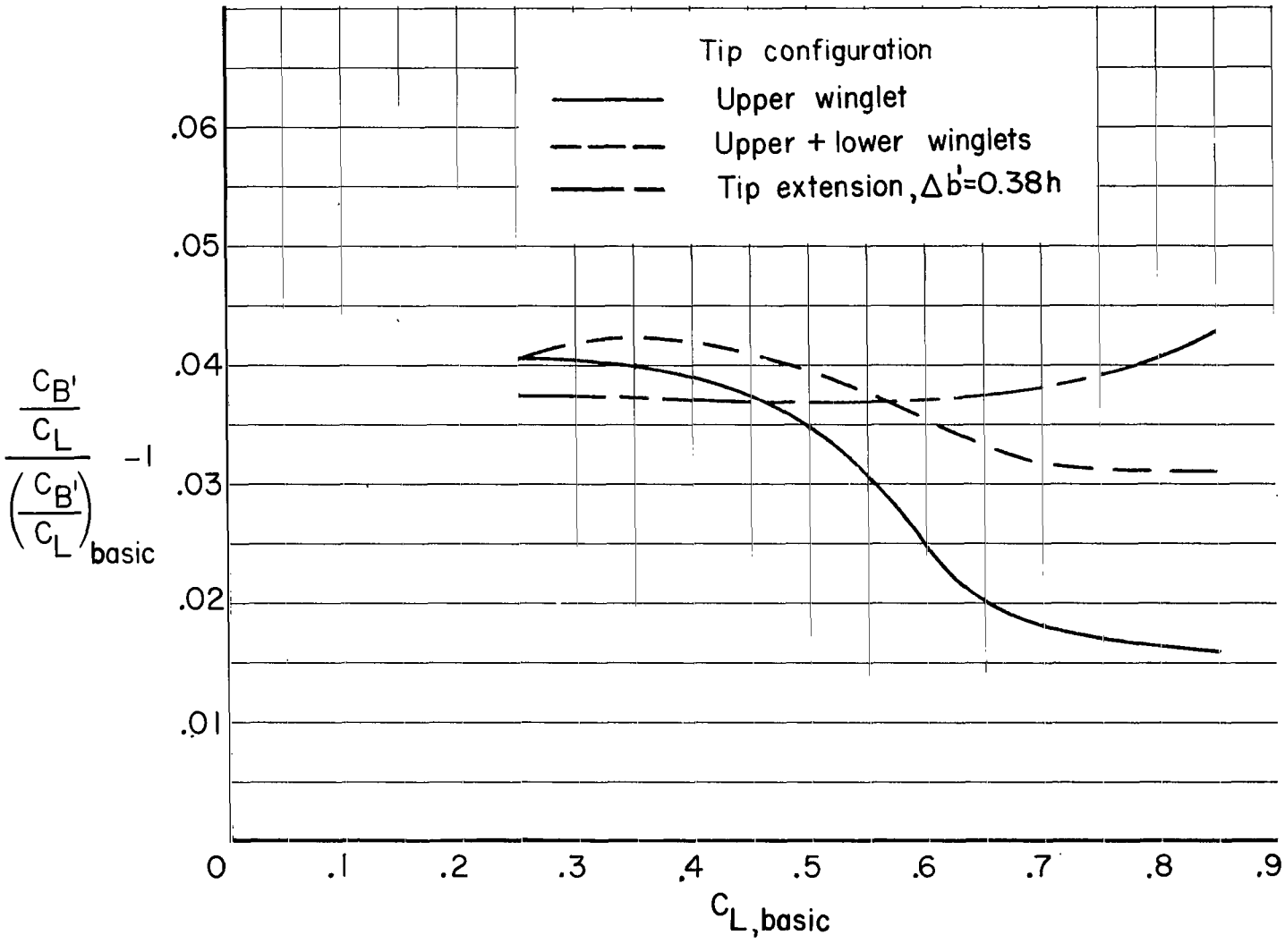

(a) $M_\infty = 0.70$.

Figure 9.- Variation of incremental bending-moment coefficient with lift coefficient.

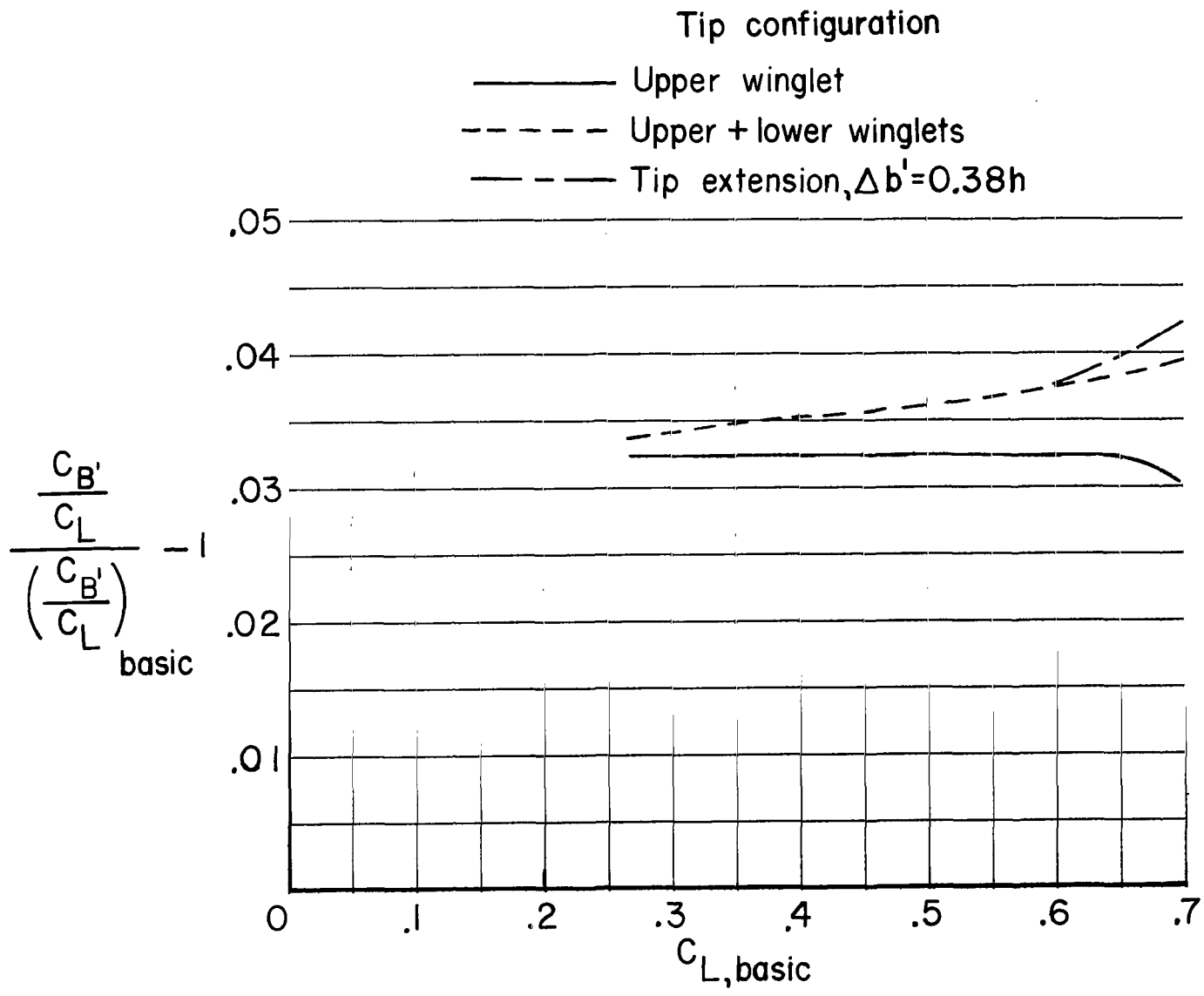

(b) $M_\infty = 0.78$.

Figure 9.- Concluded.

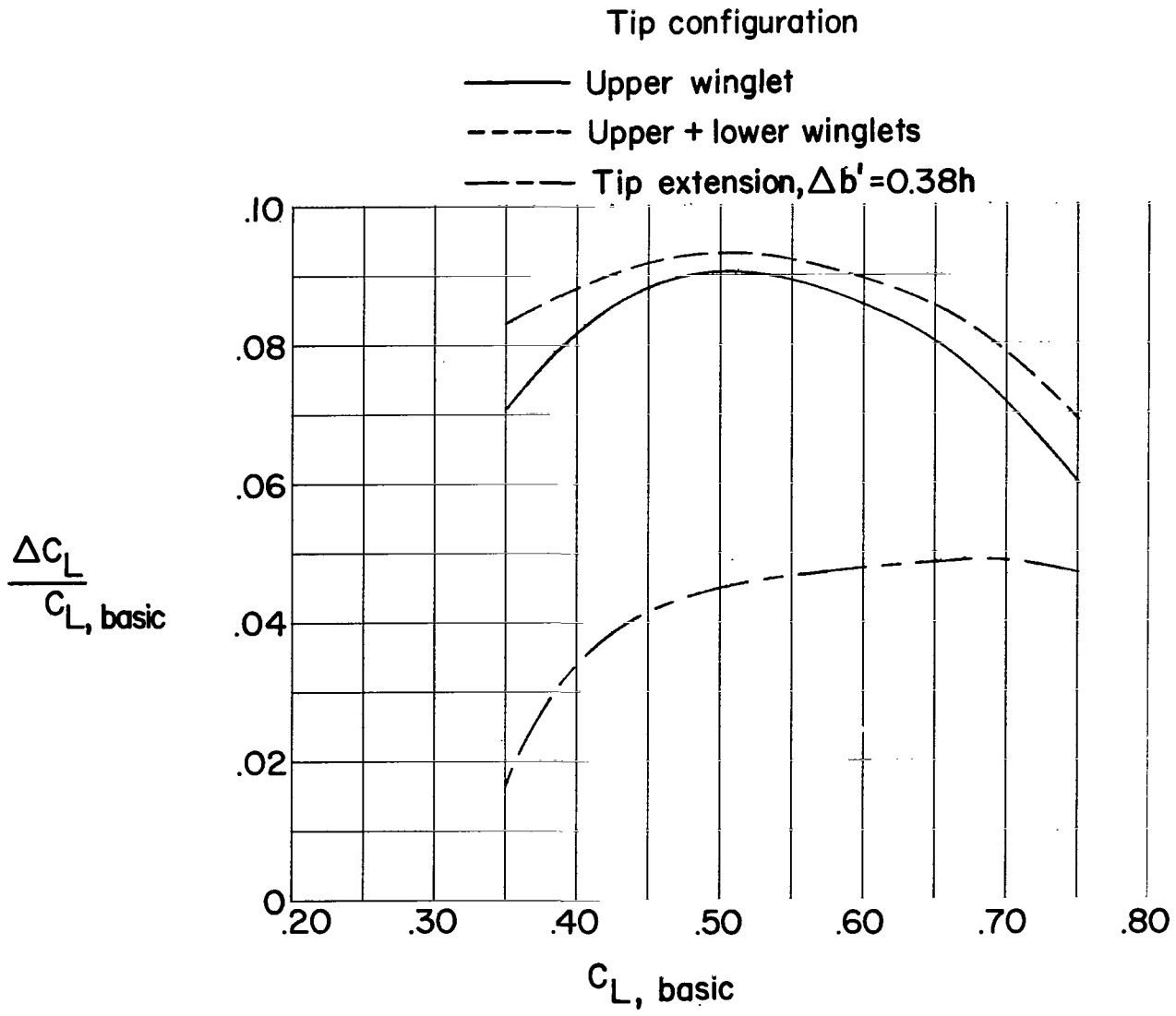

(a) $M_\infty = 0.70$.

Figure 10.- Variation of incremental lift coefficient for constant drag coefficient with lift coefficient.

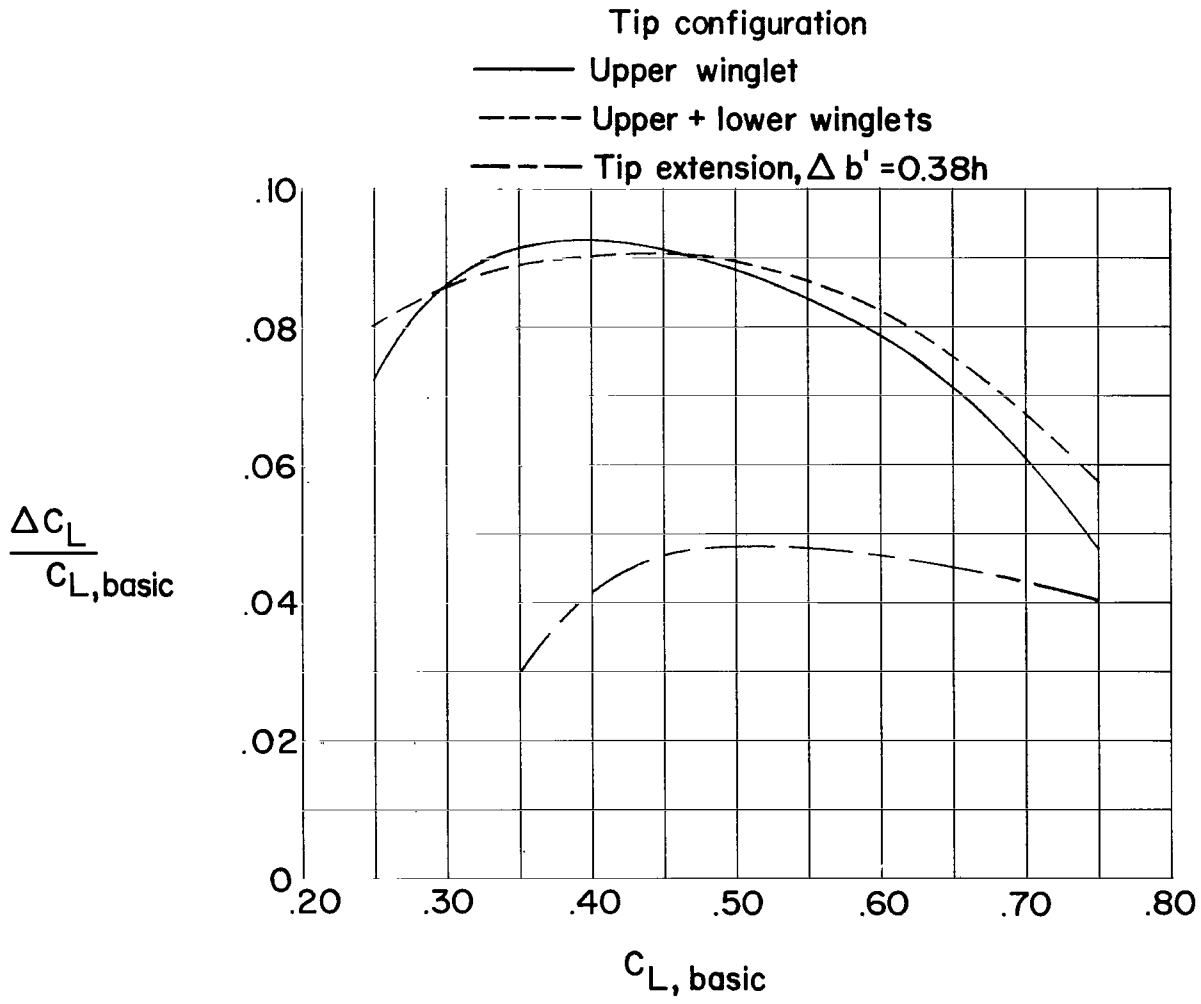

(b) $M_\infty = 0.75$.

Figure 10.- Continued.

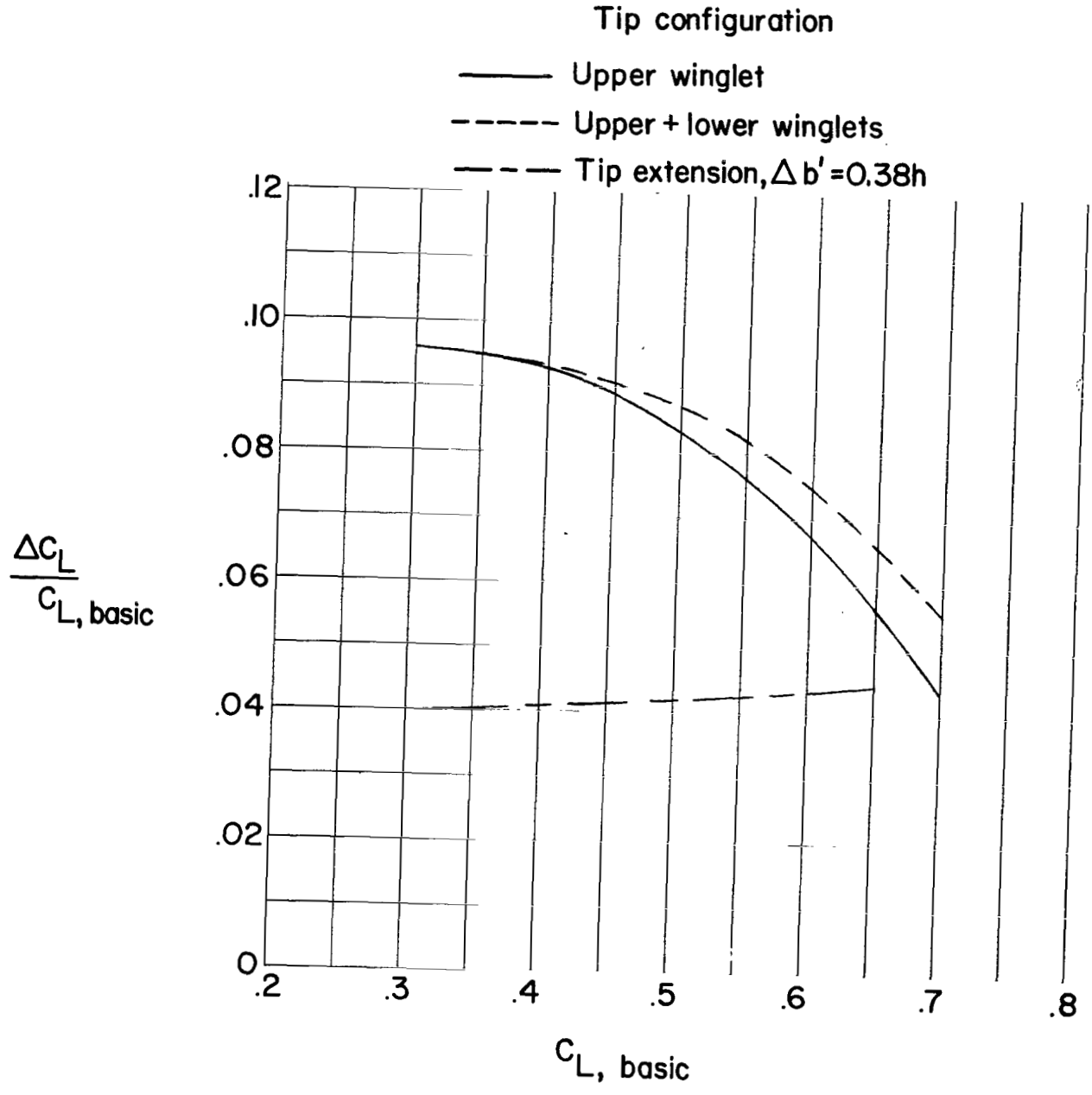

(c) $M_\infty = 0.78$.

Figure 10.- Continued.

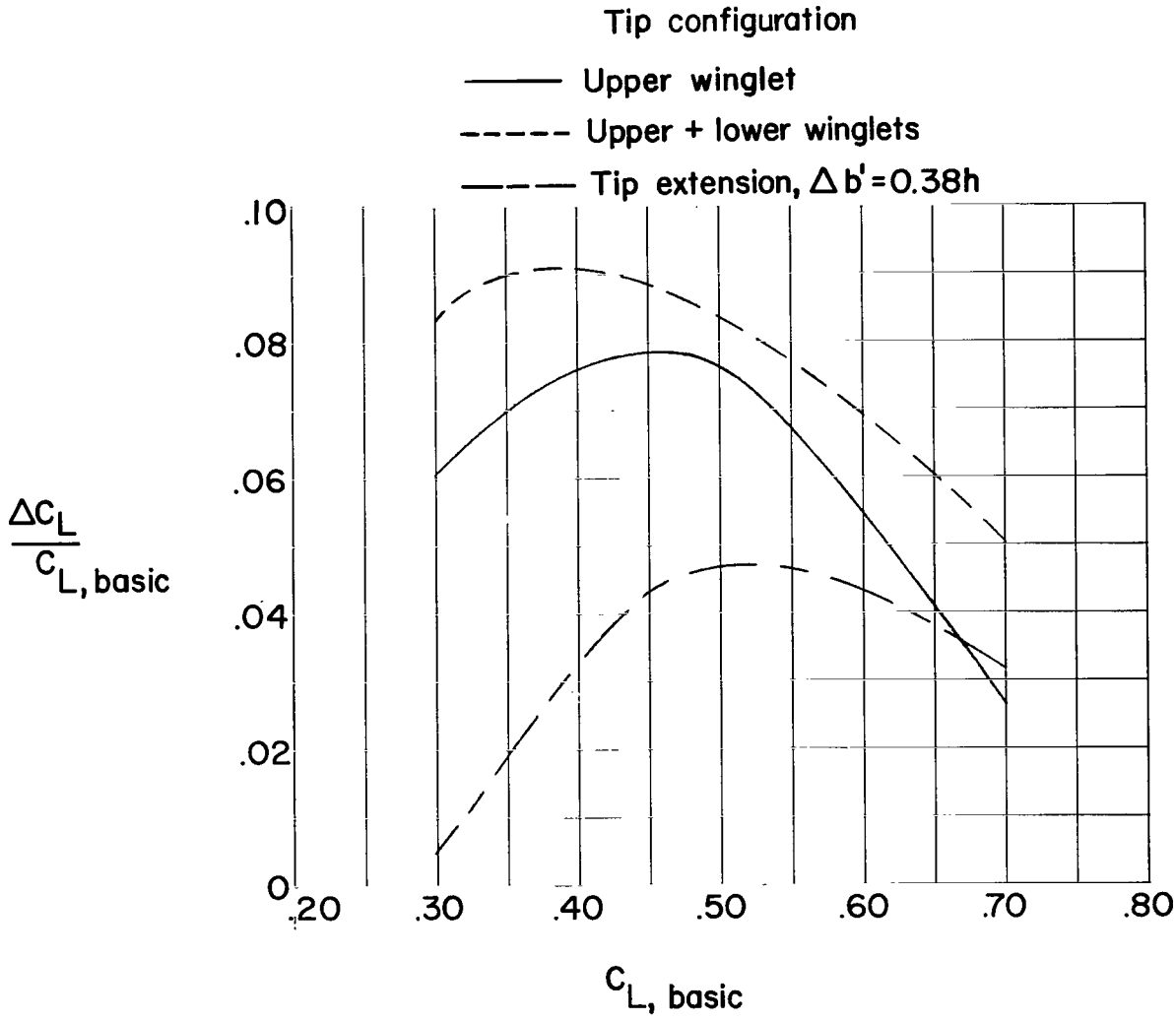

(d) $M_\infty = 0.80$.

Figure 10.- Concluded.

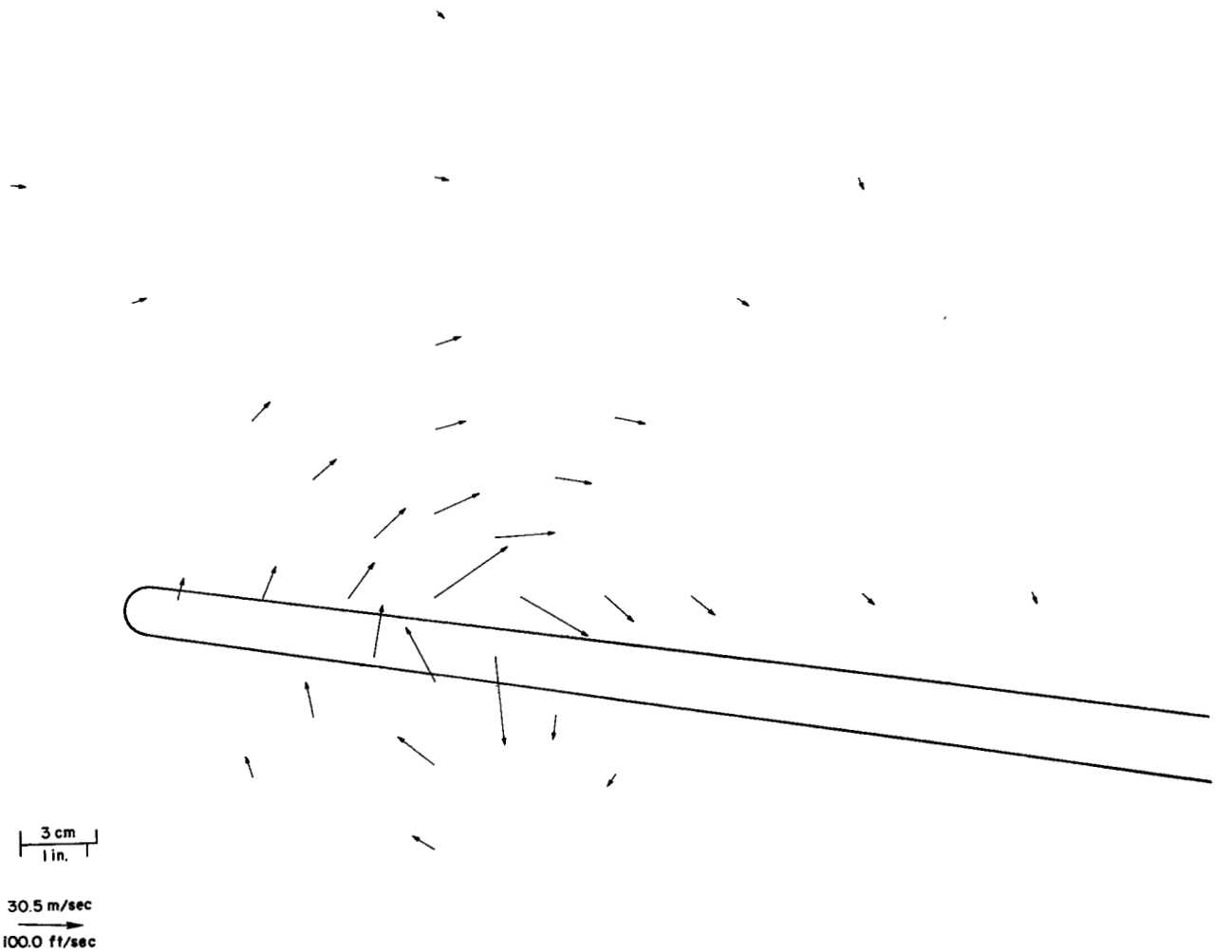

(a) Basic tip; $M_\infty = 0.70$; $C_L \approx 0.46$.

Figure 11.- Flow-field cross-flow velocity vectors downstream of wing tip.

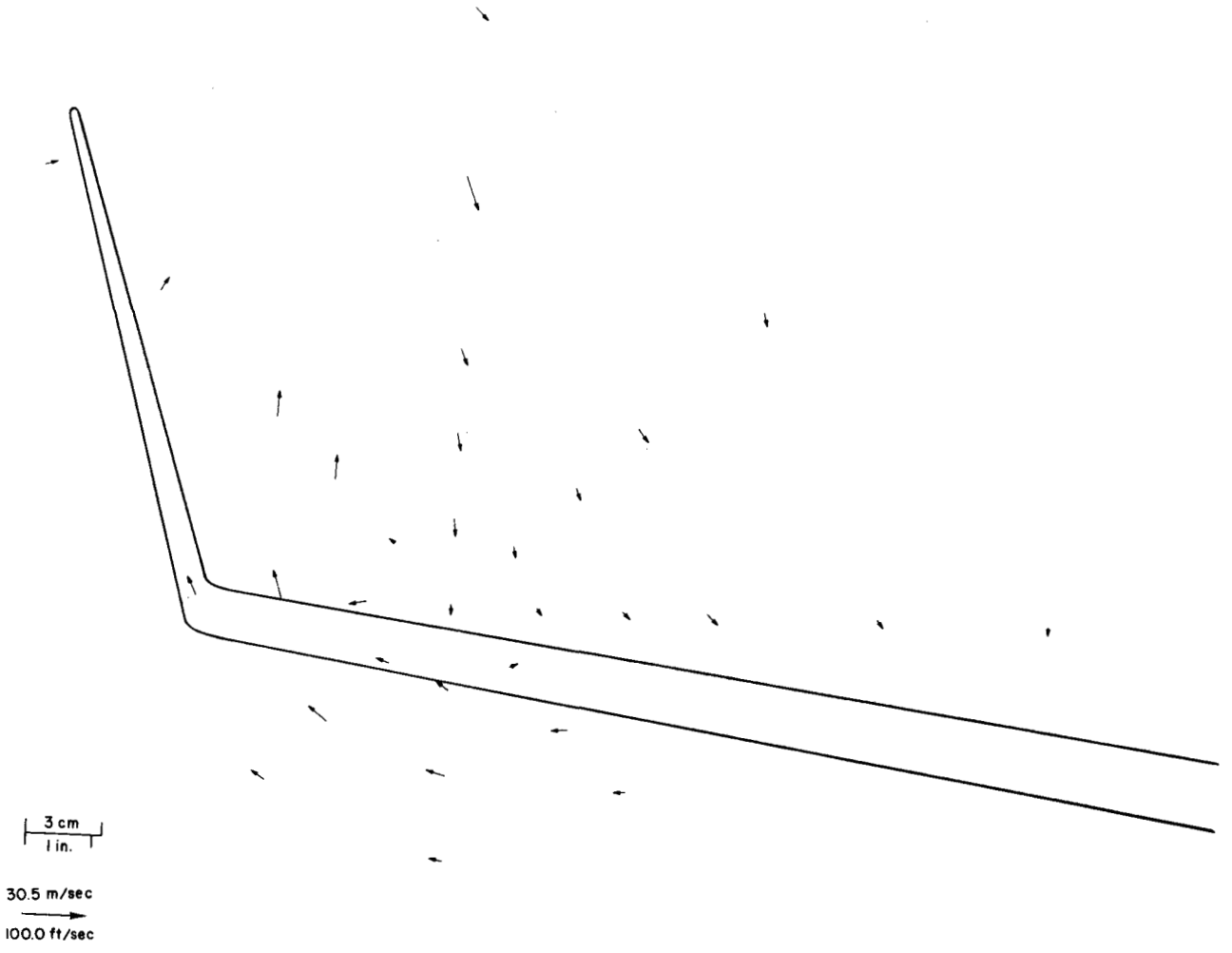

(b) Upper winglet; $M_\infty = 0.70$; $C_L \approx 0.46$.

Figure 11.- Continued.

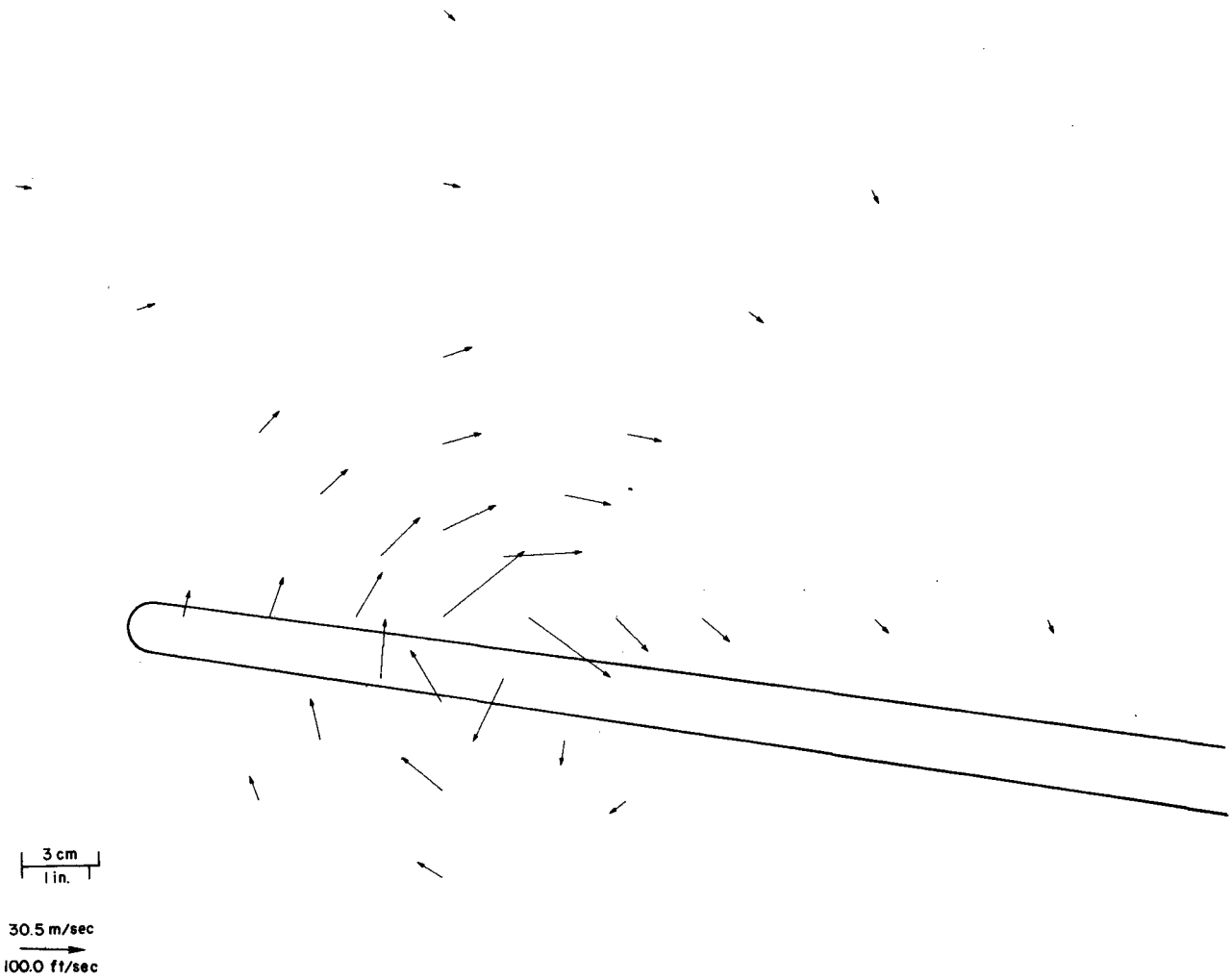

(c) Basic tip; $M_\infty = 0.78$; $C_L \approx 0.48$.

Figure 11.- Continued.

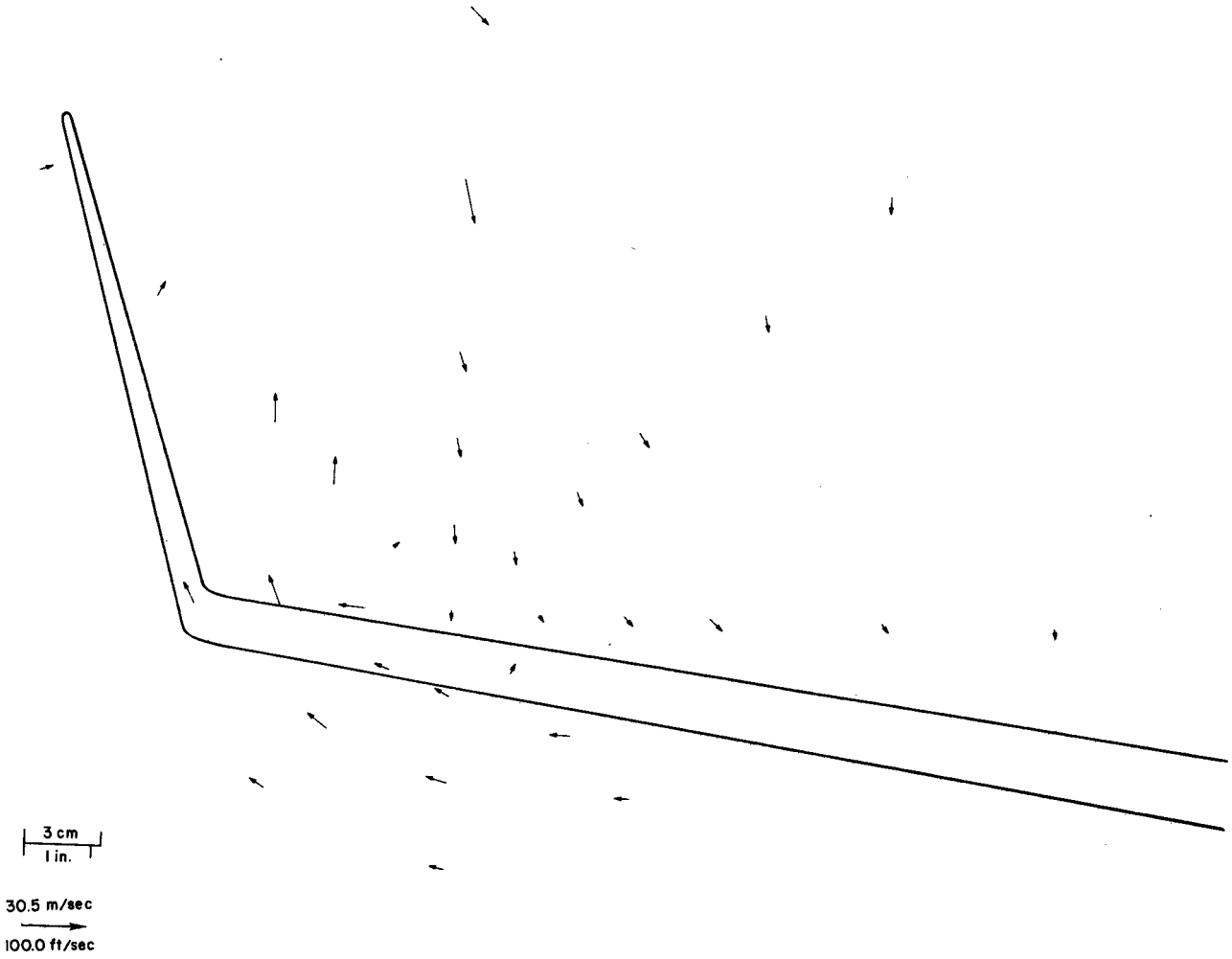

(d) Upper winglet; $M_\infty = 0.78$; $C_L \approx 0.48$.

Figure 11.- Concluded.

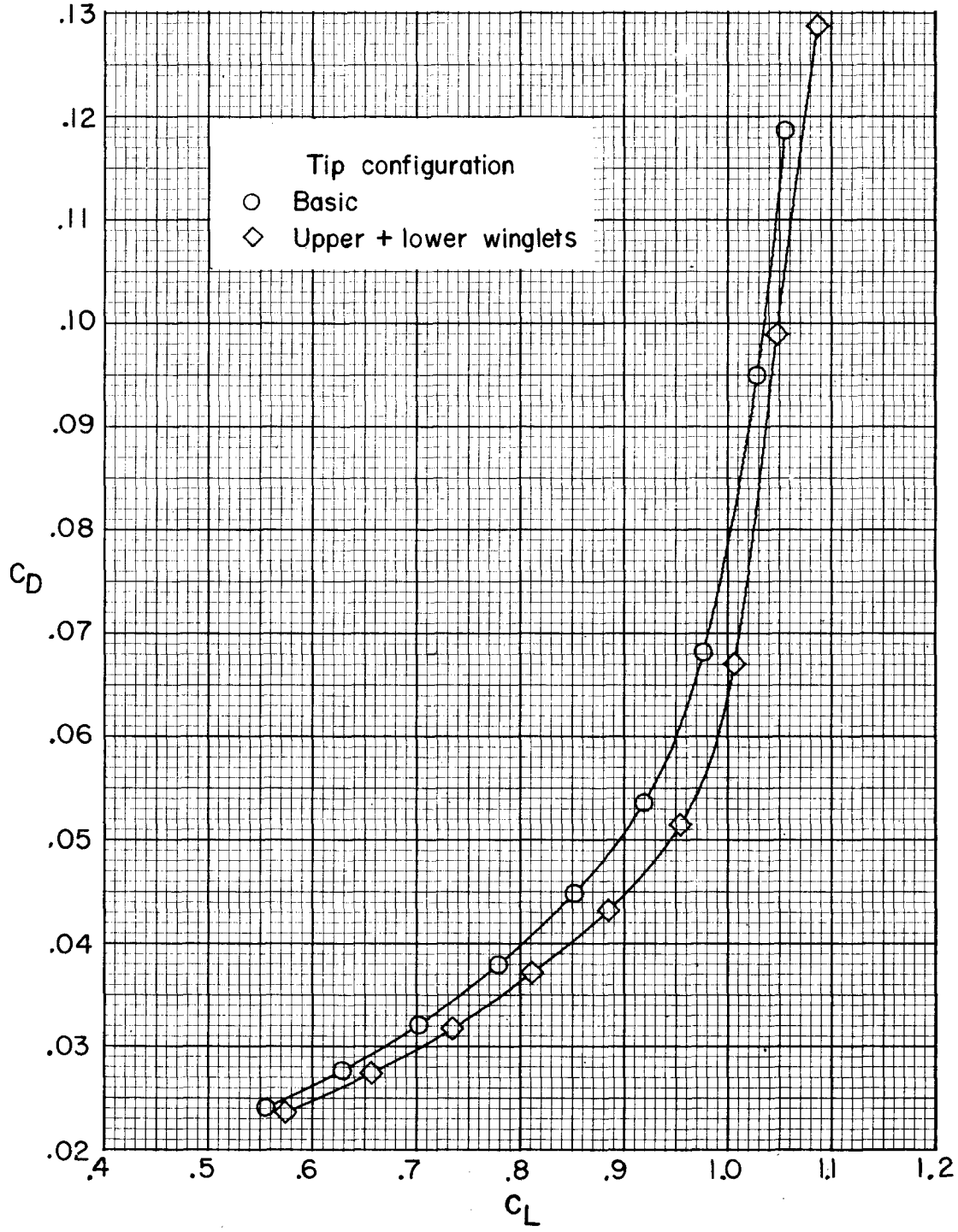

(a) No flaps.

Figure 12.- Variation of drag coefficient with lift coefficient. $M_\infty = 0.30$.

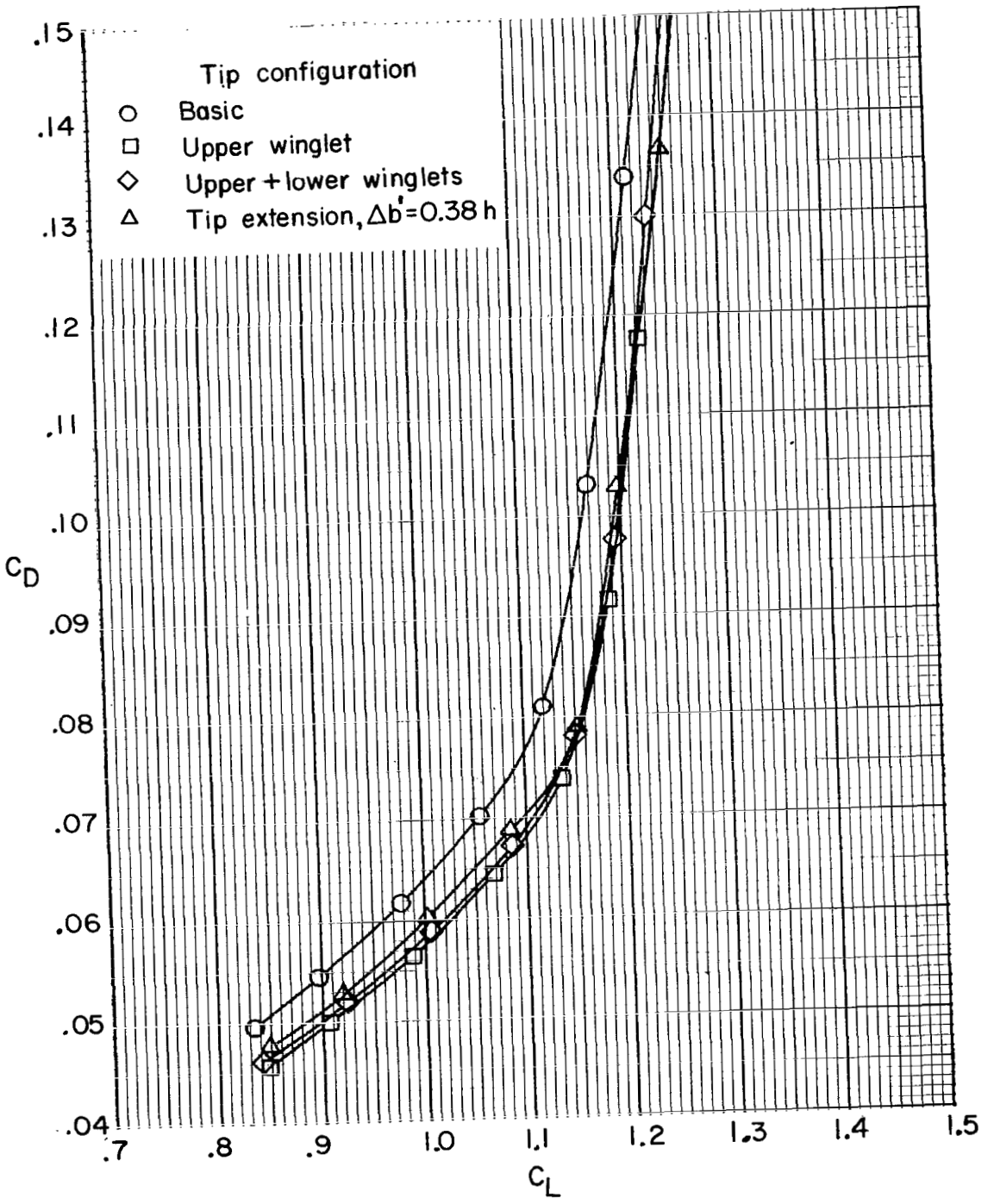

(b) Trailing-edge flaps.

Figure 12.- Continued.

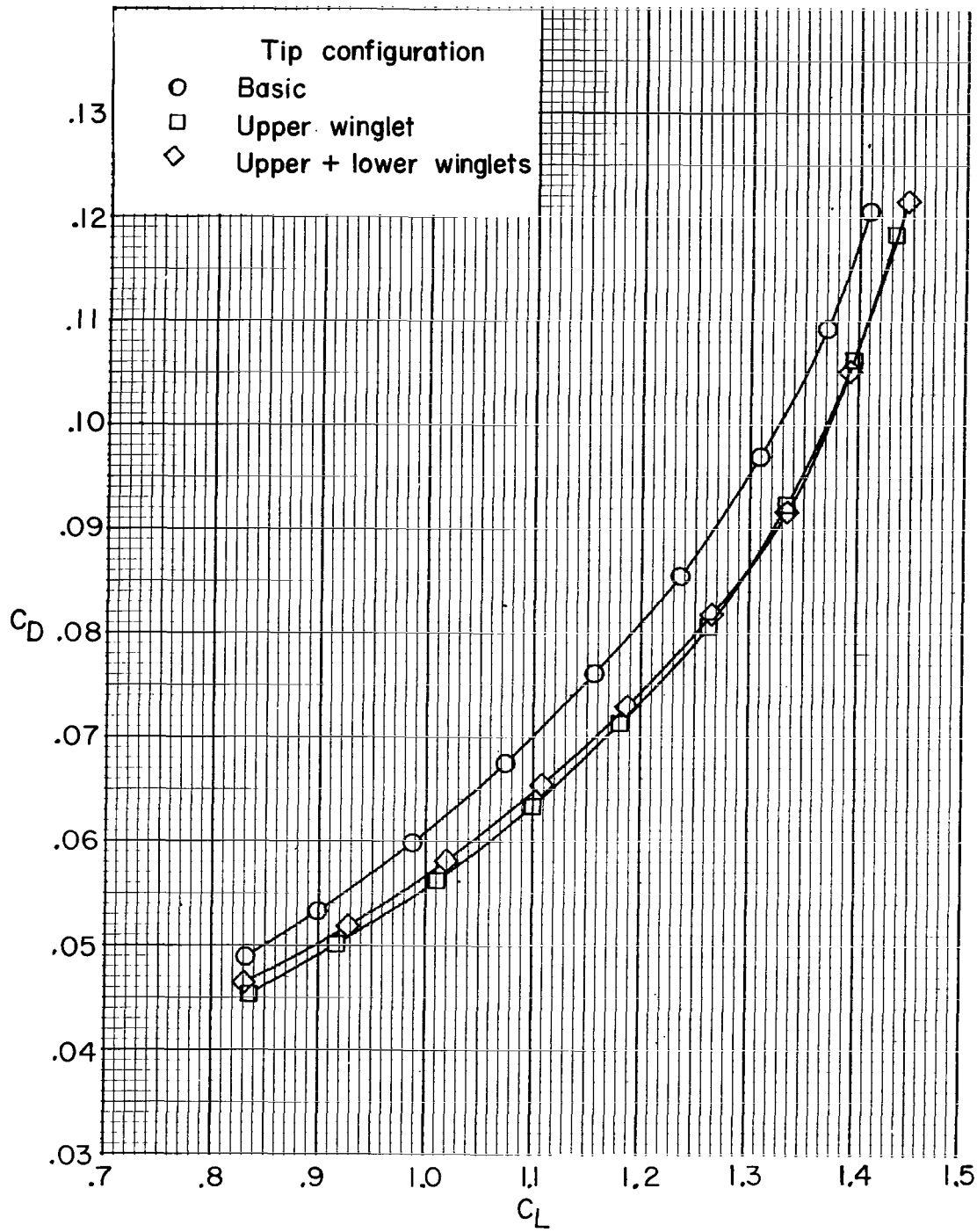

(c) Leading- and trailing-edge flaps.

Figure 12.- Concluded.

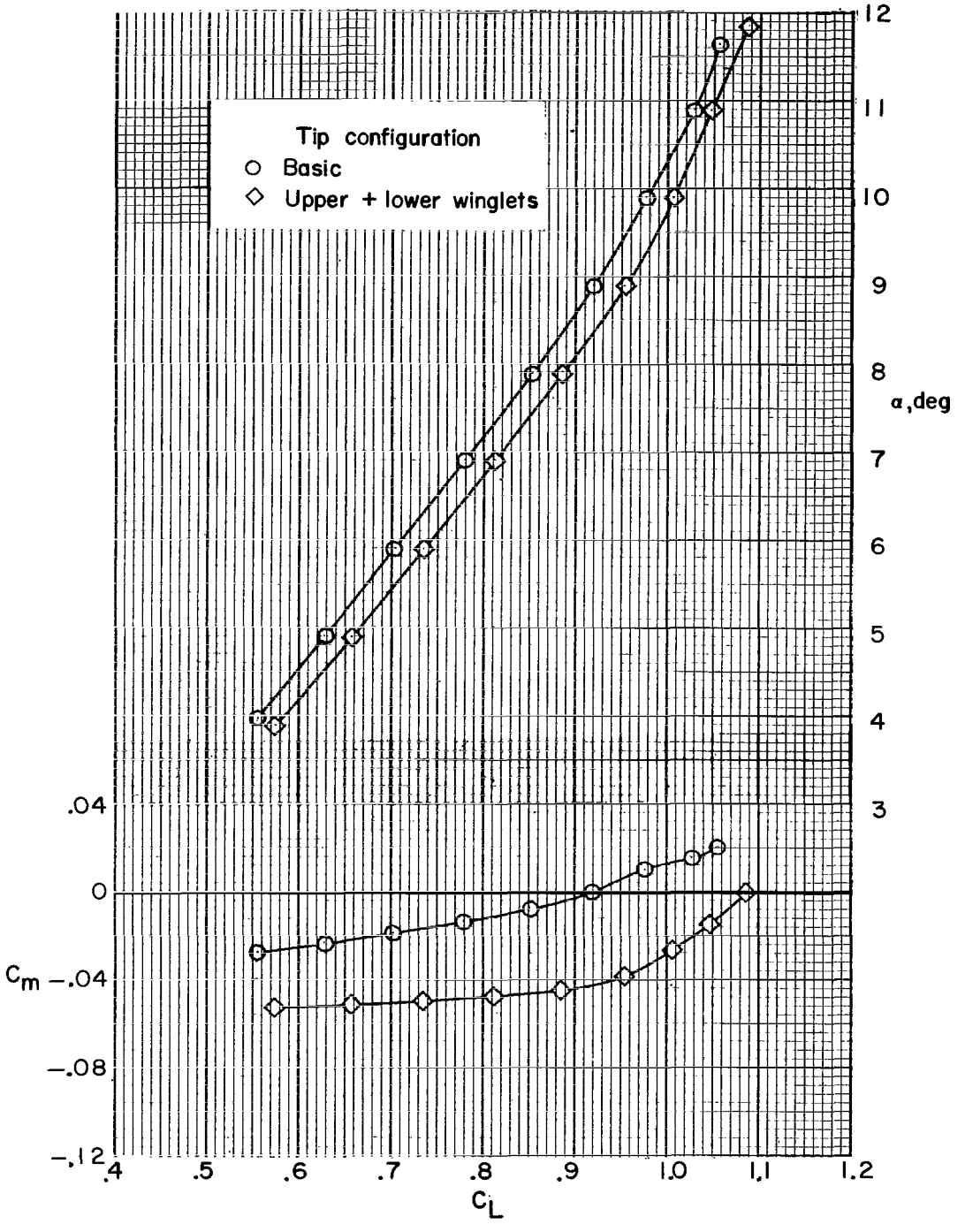

(a) No flaps.

Figure 13.- Variation of pitching-moment coefficient and angle of attack with lift coefficient. $M_\infty = 0.30$.

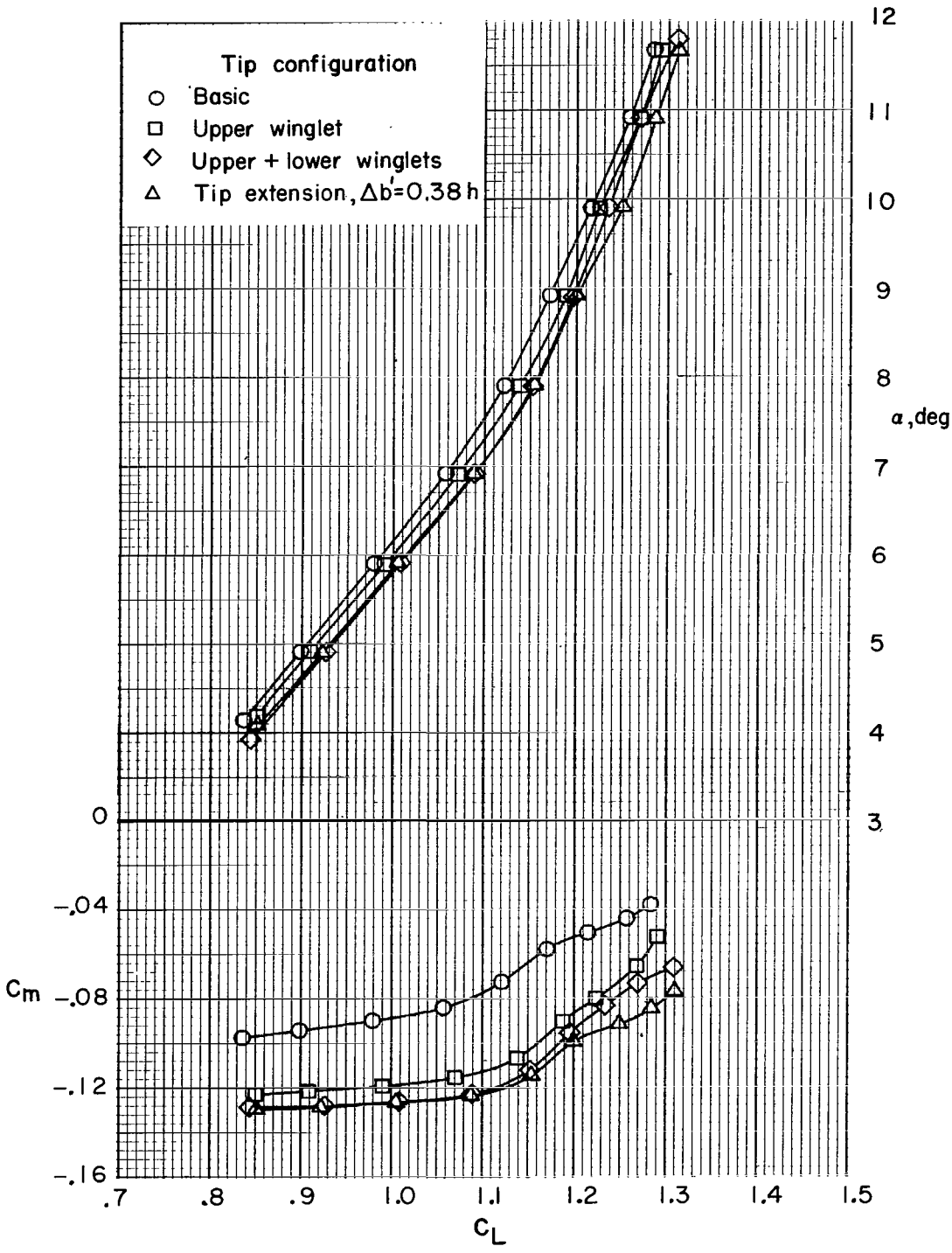

(b) Trailing-edge flaps.

Figure 13.- Continued.

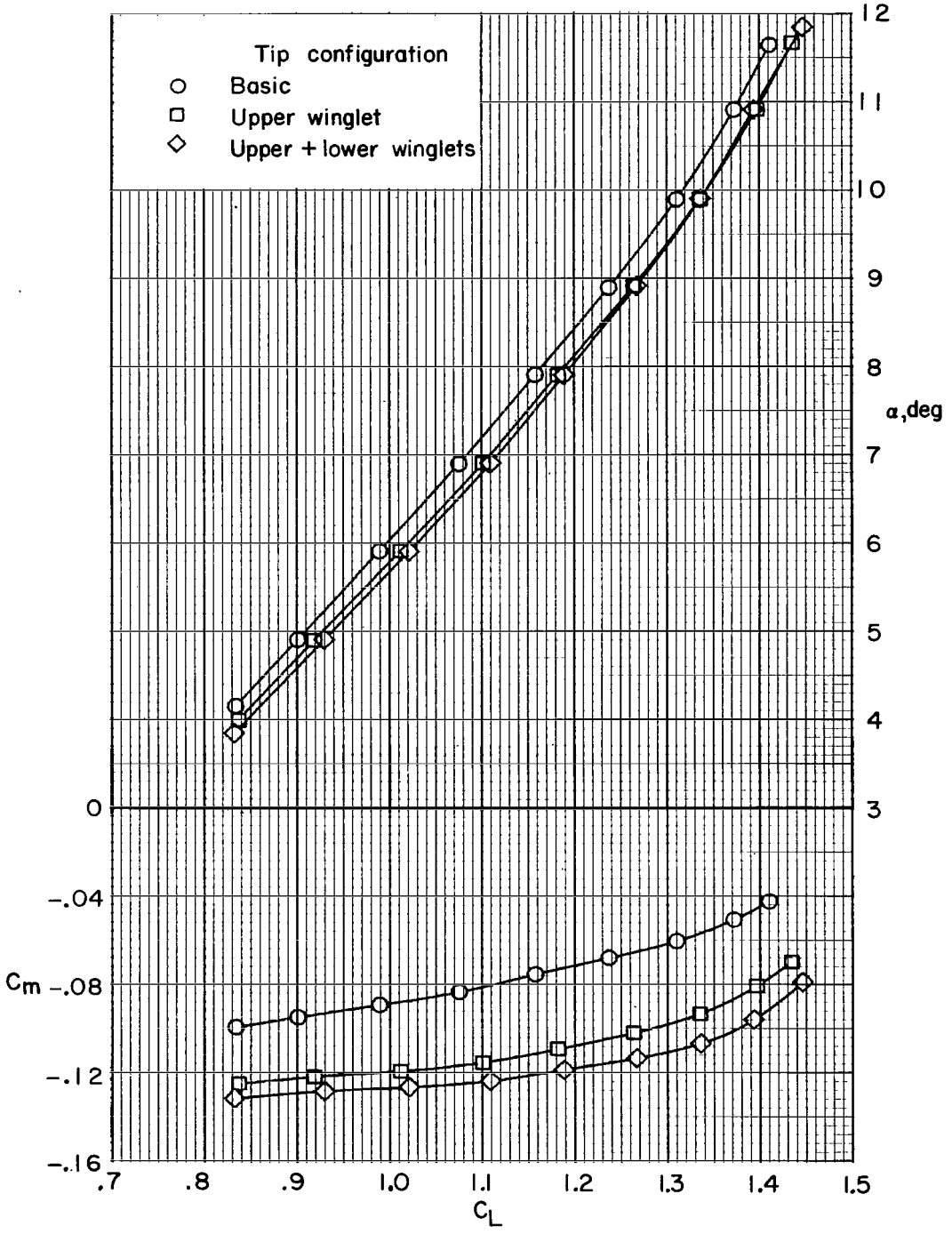

(c) Leading- and trailing-edge flaps.

Figure 13.- Concluded.

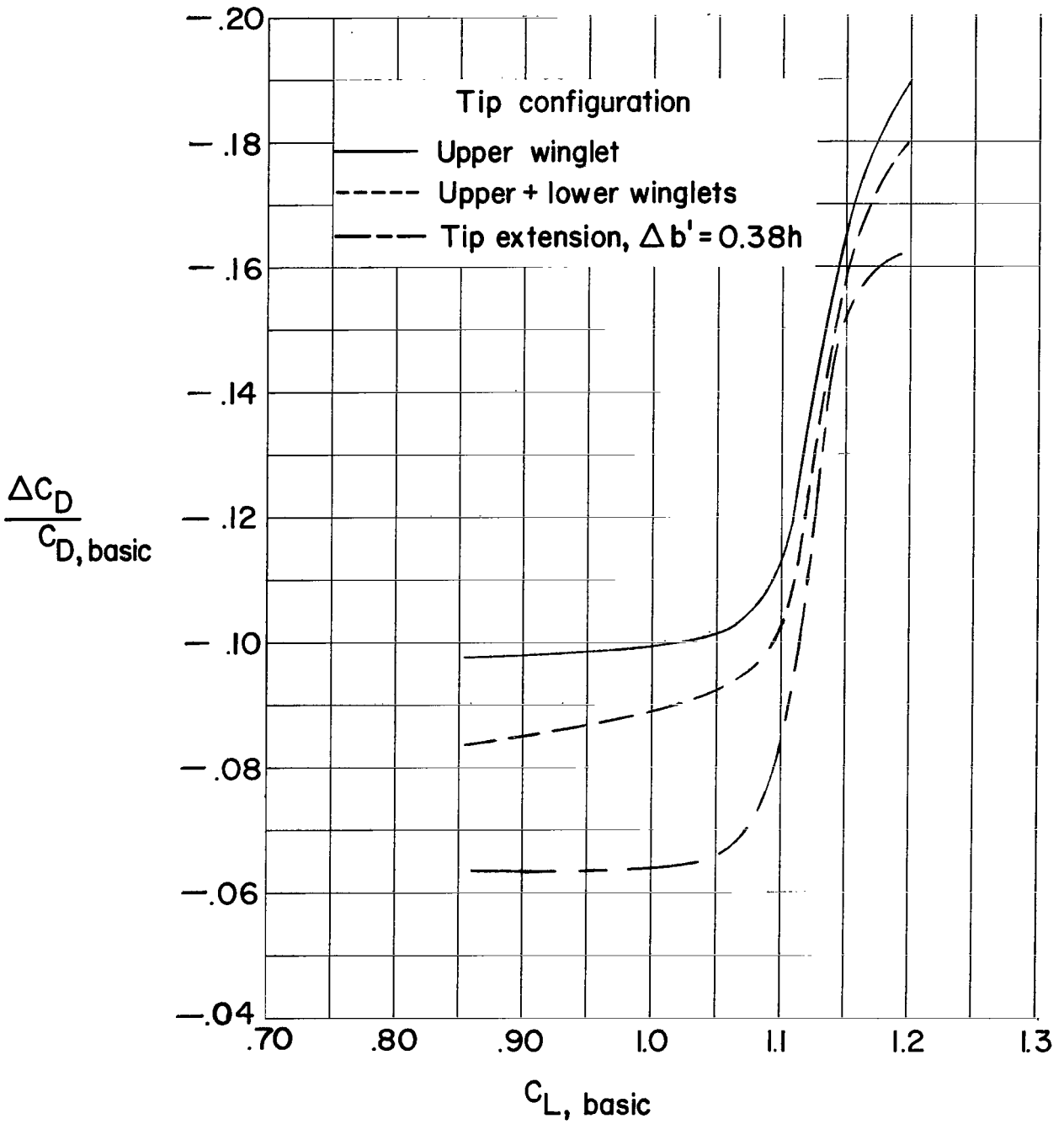

Figure 14.- Variation of incremental drag coefficient with lift coefficient. $M_\infty = 0.30$.

NATIONAL AERONAUTICS AND SPACE ADMINISTRATION
WASHINGTON, D.C. 20546

OFFICIAL BUSINESS
PENALTY FOR PRIVATE USE $300

SPECIAL FOURTH-CLASS RATE
BOOK

POSTAGE AND FEES PAID
NATIONAL AERONAUTICS AND
SPACE ADMINISTRATION
451

411 CC1 C1 U A 770603 S00903DS
DEPT OF THE AIR FORCE
AF WEAPONS LABORATORY
ATTN: TECHNICAL LIBRARY (SUI)
KIRTLAND AFB NM 87117

POSTMASTER: If Undeliverable (Section 158 Postal Manual) Do Not Return

"The aeronautical and space activities of the United States shall be conducted so as to contribute . . . to the expansion of human knowledge of phenomena in the atmosphere and space. The Administration shall provide for the widest practicable and appropriate dissemination of information concerning its activities and the results thereof."

—NATIONAL AERONAUTICS AND SPACE ACT OF 1958

NASA SCIENTIFIC AND TECHNICAL PUBLICATIONS

TECHNICAL REPORTS: Scientific and technical information considered important, complete, and a lasting contribution to existing knowledge.

TECHNICAL NOTES: Information less broad in scope but nevertheless of importance as a contribution to existing knowledge.

TECHNICAL MEMORANDUMS: Information receiving limited distribution because of preliminary data, security classification, or other reasons. Also includes conference proceedings with either limited or unlimited distribution.

CONTRACTOR REPORTS: Scientific and technical information generated under a NASA contract or grant and considered an important contribution to existing knowledge.

TECHNICAL TRANSLATIONS: Information published in a foreign language considered to merit NASA distribution in English.

SPECIAL PUBLICATIONS: Information derived from or of value to NASA activities. Publications include final reports of major projects, monographs, data compilations, handbooks, sourcebooks, and special bibliographies.

TECHNOLOGY UTILIZATION PUBLICATIONS: Information on technology used by NASA that may be of particular interest in commercial and other non-aerospace applications. Publications include Tech Briefs, Technology Utilization Reports and Technology Surveys.

Details on the availability of these publications may be obtained from:

SCIENTIFIC AND TECHNICAL INFORMATION OFFICE

NATIONAL AERONAUTICS AND SPACE ADMINISTRATION

Washington, D.C. 20546